The International Journal of Advanced Manufacturing Technology
https://doi.org/10.1007/s00170-024-13140-7

ORIGINAL ARTICLE

Impact of process parameters on improving the performance of 3D printed recycled polylactic acid (rPLA) components

Mohammad Raquibul Hasan[1] · Ian J. Davies[2] · Alokesh Pramanik[2] · Michele John[1] · Wahidul K. Biswas[1]

Received: 8 September 2023 / Accepted: 26 January 2024

Abstract

The main goal of this research was to investigate the influence of additive manufacturing (AM) printing parameters on the mechanical properties and surface roughness of specimens fabricated using recycled polylactic acid (rPLA). In order to achieve this goal, significant printing parameters such as layer thickness, infill density, and nozzle temperature were selected based on prior research. A three-level L9 orthogonal array, based on the Taguchi method, was used in the experimental design. The mechanical properties of virgin PLA and recycled PLA printed specimens were examined and compared. To facilitate the analysis of variance (ANOVA) examination, the response data for mechanical and surface roughness parameters were transformed to signal-to-noise (*S/N*) ratios. The inspected responses under consideration were the surface roughness, shore D hardness, tensile strength, flexural strength, and impact strength. The main findings suggest that careful consideration of the layer height is crucial for achieving optimum mechanical properties in the recycled PLA specimens. Furthermore, the nozzle temperature also played an important factor that affected the mechanical and surface roughness properties of the 3D printed PLA specimens. Microscopic investigation demonstrated that the number and size of voids increased significantly when the layer thickness and temperature were low, namely, 0.1 mm and 195 ℃, respectively. Finally, the optimal combination of printing parameters for each performance characteristic was determined. Following this, a confirmation test was performed using the preferred combination of parameters, which indicated a strong correlation with the outcomes predicted statistically. The results obtained from this study revealed that recycled PLA exhibited mechanical properties comparable to that of virgin PLA under certain conditions. In summary, the results of this study will serve as a valuable dataset in the field of additive manufacturing, providing valuable insights for other researchers working with recycled PLA material.

Keywords Fused deposition modelling (FDM) · Recycled polylactic acid (recycled PLA) · Taguchi design of experiment (DoE) · Mechanical properties

1 Introduction

Technological advancements have a substantial impact on the competitiveness amongst manufacturers in various industry sectors due to the increasing demand for high-quality customised parts that are economical and have structurally sound mechanical qualities [1]. Additive manufacturing (AM) technology, also known as three-dimensional (3D) printing, has the potential to address the mentioned issues due to their design flexibility, manufacturing simplicity, lower production costs, and reduction of raw material waste [2]. These advantages make 3D printing an attractive alternative to conventional manufacturing methods [3–6]. There are several commercially available AM processes, such as inkjet modelling (IJM), fused deposition modelling (FDM), stereolithography (SLA), and laminated

✉ Mohammad Raquibul Hasan
m.hasan21@postgrad.curtin.edu.au

Ian J. Davies
i.davies@curtin.edu.au

Alokesh Pramanik
alokesh.pramanik@curtin.edu.au

Michele John
m.rosano@curtin.edu.au

Wahidul K. Biswas
w.biswas@curtin.edu.au

[1] Sustainable Engineering Group, School of Civil and Mechanical Engineering, Curtin University, Bentley, WA 6102, Australia

[2] School of Civil and Mechanical Engineering, Curtin University, Bentley, WA 6102, Australia

Published online: 20 February 2024

object manufacturing (LOM). However, FDM stands out as a widely utilised technology that involves the extrusion of semi-solid thermoplastic materials through a nozzle in contrast to other AM techniques that employ diverse laser systems, powders, and resins [7–9]. The FDM process has the capability to construct complex geometries using lightweight materials, resulting in a notable reduction in processing time [10, 11].

A range of thermoplastic polymer materials, such as polylactic acid (PLA), polyethylene terephthalate (PET), acrylonitrile–butadiene styrene (ABS), polypropylene (PP), and high-density polyethylene (HDPE), are the most extensively documented polymers employed in the FDM process [12–14]. Amongst these polymers, PLA has attracted considerable interest as a bio-based and biodegradable polymer that serves as a viable substitute for petroleum-derived plastics [15]. PLA exhibits a relatively lower molecular weight and low melting point, rendering it highly compatible with a wide range of FDM equipment [14, 16]. Moreover, it has been observed that the mechanical properties of PLA exhibit a higher level of performance when compared to ABS and PETG [17]. In addition, PLA has better recyclable properties than other thermoplastic polymers [18]. By considering limited material resources and the relatively high price of virgin polymers, future recycling of PLA could become economically attractive. Therefore, recycling of PLA for 3D printing could be a feasible option, as it offers environmental benefits and comparable mechanical characteristics [19].

Previous research has indicated that the recycling process is subject to a high shear force and temperature, which facilitate chain scission processes. This causes a reduction in the molecular weight and viscosity, which ultimately reduces the mechanical strength hindering the use of recycled PLA (rPLA) [3, 20]. Furthermore, the anisotropic characteristics of FDM produce pores, which reduce its strength and other important characteristics [21]. As a consequence, whilst the utilisation of virgin PLA (vPLA) in the context of 3D printing has been extensively documented in the academic literature, the application of recycled PLA remains relatively uncommon. Hence, proper use of recycled materials is important towards the efficacy of recycled plastic materials and green manufacturing techniques.

According to existing research, the overall mechanical performance of printed specimens can be improved by modifying various printing parameters, such as the nozzle/extrusion temperature, layer thickness/height, nozzle diameter, infill percentage, infill pattern, printing speed, build orientation (flat, edge, and upright), raster/infill orientation, and top and bottom layer thicknesses [3, 17, 22]. Therefore, it is essential to optimise and control all these factors effectively within the FDM manufacturing process to fabricate components with higher dimensional precision and enhanced mechanical functionality [23]. Several studies have been conducted to improve the mechanical properties of rPLA by changing the process parameters. Dey et al. [24] altered the infill percentage, layer thickness, printing speed, nozzle temperature, build orientation, and raster angle to modify the mechanical properties of recycled PLA and observed an increase. Atakok et al. [17] conducted an experiment using a commercially recycled PLA filament to examine the impact of the layer thickness, infill percentage, and infill pattern on the mechanical properties. The findings of the investigation indicated that employing a layer thickness of 0.25 mm and an infill percentage of 70% yielded mechanical properties that closely resembled those of the vPLA. Correia et al. [25] determined that by utilising the optimal combination printing parameters, such as 0.2 mm layer thickness, 100% infill, and 40 mm/s travel speed, would effectively improve the mechanical properties of rPLA. In their study, Tan et al. [22] determined that the optimal printing parameters for enhancing the tensile strength and flexural strength of recycled polylactic acid (rPLA) include a fan cooling speed of 100%, an extruder temperature of 190 °C, and a bed temperature of 50 °C. Breški et al. [26] assessed that 30% infill and 0.1 mm layer thickness were most favourable for higher mechanical properties of rPLA. These studies showed that different infill percentages and layer thicknesses can improve the mechanical properties of rPLA 3D printed parts. Therefore, modification and optimisation of different printing parameters can improve the overall mechanical properties [27].

Numerous researchers have attempted to investigate the impact of the process parameters on the behaviour of 3D printed vPLA components. Lanzotti et al. [28] conducted a study to examine tensile properties of 3D printed PLA components by varying the layer thickness and build orientation. The findings of this study demonstrated that a decrease in layer thickness resulted in the attainment of the highest ultimate tensile strength. Eryildiz [29] experimentally determined that a flat orientation showed higher tensile properties compared to the upright build orientation due to the intralayer and interlayer phenomena. Benamira et al. [30] also printed tensile specimens in a flat position and observed improved tensile properties. Tsouknidas et al. [31] examined the influence of various printing speeds on the compressive strength of the PLA samples and concluded that by lowering the printing speeds, maximum strength could be achieved. In their study, Carneiro et al. [32] investigated parameters such as the infill density, layer thickness, and raster orientation and found that the layer thickness had the least impact on the mechanical properties. In their study, Kam et al. [33] found that the infill percentage directly influenced the tensile and Izod impact strengths of PLA parts. This study identified a significant positive correlation between strength and infill percentage. In a study conducted by Suteja and Soesanti [34], it was observed that the layer thickness had a notable impact on the tensile strength. Behzadnasab et al. [35]

observed that increasing nozzle temperature from 180 to 240 °C increased mechanical strength in PLA 3D printed parts. Finally, Sun et al. [36] demonstrated that the bed temperature plays a crucial role in the bonding process, consequently leading to an enhancement in the tensile strength.

Regarding the optimization of printing parameters, researchers have utilised a range of design of experiments (DoE) methods, including full factorial design (FFD), fuzzy logic (FL), response surface methodology (RSM), central composite design (CCD), analysis of variance (ANOVA), and the Taguchi method [10, 21, 37, 38]. Several recently published studies have focused on optimising 3D printing process parameters using DoE methods. In their research, Chari et al. [39] examined the compressive strength and hardness of 3D printed PLA components by using the Taguchi method with varying nozzle temperature, infill, and layer thickness. Heidari-Rarani et al. [37] employed the Taguchi DoE method to examine the mechanical properties of PLA specimens by modifying infill density, print speed, and layer thickness. This study found that the impact of the infill density on the mechanical characteristics was significantly greater than that of the printing speed and layer thickness. To determine the impact of printing factors on the mechanical strength of FDM printed specimens, Sood et al. [40] used CCD for DoE and utilised ANOVA to optimise printing settings. The Taguchi approach was used by Alafaghani et al. [41] to investigate the impact of the infill pattern and percentage, layer thickness, and nozzle temperature on the characteristics of specimens made using PLA filaments. By utilising this approach, researchers aimed to gain insights into the optimal combination of these parameters to enhance the overall quality of the fabricated specimens. Therefore, the selection and optimisation of the FDM parameters are essential for achieving the desired technical properties of 3D printed components.

A review of the sources mentioned above indicates that recent scientific investigations have focused on analysing the influence of various factors on the mechanical strength of vPLA printed specimens, such as layer thickness, infill density, infill pattern, print speed, build orientation, and nozzle temperature. However, the mechanical strength of rPLA still remains unexplored. Additionally, no previous research has investigated the impact of layer height, infill density, and nozzle temperature on rPLA 3D printed specimens, and this is considered a novelty of the present work. Thus, it is necessary to conduct an in-depth analysis of the effects of layer height, infill density, and nozzle temperature on the performance of rPLA in order to achieve optimal outcomes and provide significant statistical information for future researchers in the field. Therefore, this study is aimed at assessing the mechanical properties of FDM manufactured samples utilising virgin and recycled PLA materials by varying the layer height, infill density, and nozzle temperature. This study will guide the researchers and encourage the manufacturing company to fabricate products for engineering applications using recycled PLA. This study employs the design of experiments (DOEs) technique to investigate the impact of selected printing parameters on the surface roughness, hardness, tensile, flexural, and impact strengths. In addition, confirmation tests were conducted to validate the optimal process parameters obtained by the DoE technique in order to propose the most appropriate printing parameter as a viable manufacturing protocol for future process optimisation.

2 Materials and methods

The main objective of this study was to investigate a preferred combination of 3D printing parameters to optimise the mechanical properties of virgin PLA and recycled PLA specimens using the Taguchi method. The proposed methodology followed in the work has been shown in Fig. 1.

As a first step, the experimental setup was planned and prepared, wherein the control parameters for 3D printing were carefully chosen. The range of the control parameters was selected, specific levels were assigned to each parameter, and then a Taguchi orthogonal array was chosen. After the initial stage, experiments were conducted using the Taguchi method. The experimental data were statistically analysed in the form of average values, *S/N* ratios, main effect plots, and analysis of variance (ANOVA). Finally, the optimal values for each control parameter were identified, and the optimised results were subsequently validated through confirmation experiments. A comprehensive description of the materials, printing parameter selection, testing conditions, and analysis employed in the production and characterisation of the samples will be provided in the subsequent subsections.

2.1 Materials

Polylactic acid is one of the most commonly used thermoplastics for fused deposition modelling due to its favourable printing properties and ease of use as a filament in 3D printing [17]. This biodegradable, thermoplastic material originates from cleaner sources when compared to conventional plastics, with less hazardous components, and can be printed at lower temperatures saving energy [4]. PLA has a melting point of approximately 150–160 °C, can be easily processed at 190–230 ℃, and has a high tensile strength of 50–60 MPa when compared to ABS and PET [42]. For this study, virgin PLA and recycled PLA (recycled from residual extrusion waste stream, which are subsequently recompounded and homogenised) filaments, with 1.75 mm diameter, were purchased (X3D, Perth, Western Australia) and used without further modification, for example, no additives or thermal/chemical changes. PLA filaments can absorb moisture from

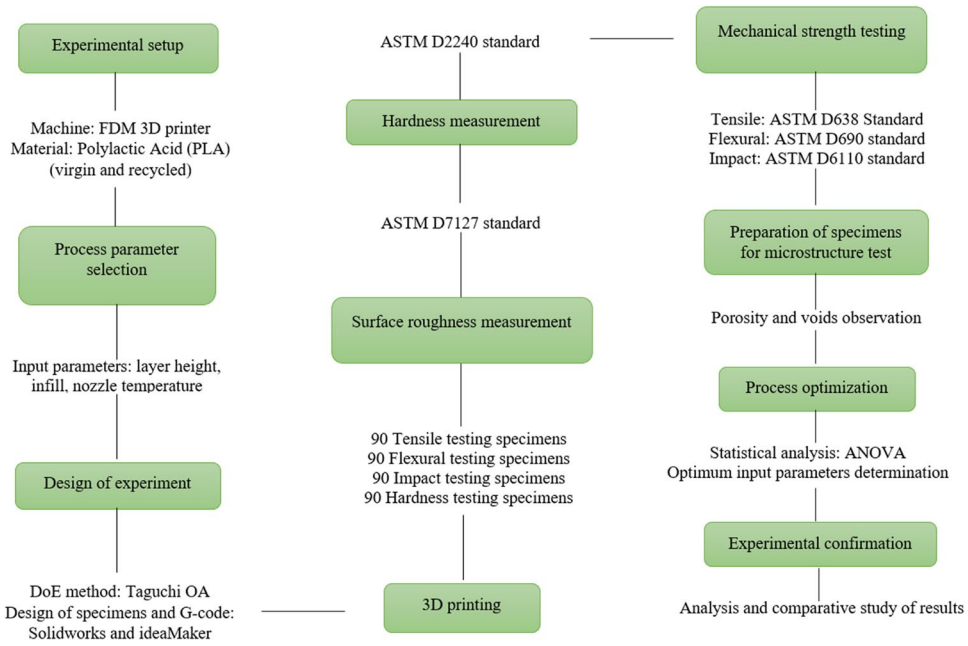

Fig. 1 Flow diagram of the research methods followed in the present work

their surroundings, which can impair the quality of printed specimens [43]. Filaments were stored in plastic desiccators containing silica gel in order to avoid moisture adsorption prior to their use.

2.2 Selection of printing parameters

The mechanical properties of FDM printed parts are known to be influenced by several printing parameters. The literature review noted that different printing parameters had been taken into consideration by previous researchers to improve the mechanical properties of 3D printed PLA parts, including layer thickness, shell, infill percentage, infill pattern, nozzle temperature, print speed, and print orientation [13, 14, 33, 44, 45]. Therefore, based on earlier studies, parameters that directly impacted mechanical properties and surface roughness, such as infill density, layer thickness, and nozzle temperature, were chosen for this study across three levels.

The choice of the factors and their corresponding levels was motivated by the interest in maintaining the printing quality and mechanical performance of 3D printed components. The first input parameter considered was the layer height, which measures the individual layer height deposited by a nozzle tip. The printing time and printing quality of a specimen could be influenced by this printing parameter [46]. Values of 0.1 mm, 0.2 mm, and 0.3 mm were chosen as being typical values for the layer height. Second, the infill density indicates the degree to which the printed part is solid or hollow, where a 0% infill is fully hollow, and a 100% is fully solid. Printing time, part cost, and mechanical strength are known to generally increase with infill density; for this reason, three levels of infill, 60%, 80%, and 100%, were selected for analysis. The final input parameter considered was the nozzle temperature (alternatively known as the printing temperature), which denotes the temperature of the extruding nozzle. Three levels of nozzle temperatures were selected at 195 ℃, 205 ℃, and 215 ℃ to analyse the strength of the bond between the layers. It is noted that 190–220 ℃ is the temperature range recommended by the manufacturer for printing. The configurations of printing parameters have been summarised in Table 1.

2.3 Experimental design using Taguchi orthogonal approach

The number of 3D printed specimens required to assess the influence of printing parameters on the mechanical properties and microstructure needed to be chosen. Therefore, it is important to organise, conduct, evaluate, and interpret tests to assess the factors that impact the value of a parameter or set of parameters. Design of experiment is a useful tool to improve the consistency of results whilst minimising the number of experiments without loss of accuracy. The DoE methodology employs orthogonal arrays (OA) to determine the optimal number of trials and their corresponding levels

Table 1 Proposed levels of 3D printing parameters for the experimental design

Factors	Level 1	Level 2	Level 3
Layer height (mm)	0.1	0.2	0.3
Infill density (%)	60	80	100
Nozzle temperature (℃)	195	205	215

[47]. Numerous types of DoE have been described in the literature, including full factorial design (FFD), central composite design (CCD), definitive screening design (DSD), Box-Behnken design (BBD), and the Taguchi method [48]. In this work, Taguchi method was selected to design the OA due to its effectiveness and ability to minimise the number of experiments performed [49]. Based on the selected parameters, an L9-OA was created using the MINITAB 21 software. The Taguchi DoE using L9-OA for the sample preparation is presented in Table 2. The array was utilised as a base for every material (vPLA and rPLA) when the test rounds were planned.

2.4 Fabrication of test samples by 3D printing

Once the L9 specifications of the specimens (Table 2) were determined for the different printing parameters, the specimens were printed according to these specifications. A Raise 3D E2 FDM printer with a nozzle diameter of 0.4 mm was used to manufacture the specimens according to the L9 orthogonal array. This printer uses the ideaMaker slicer software to slice the 3D model (STL file) and modifies the 3D printing process parameters, such as the infill type, percentage, layer thickness, heated bed temperature, and fan speed. After designing the test parts using Solidworks computer aided design (CAD) programme, the models were transformed into standard tessellation language (STL) files with linear tolerance of 0.05 mm and angular tolerance of 1° ASTM D638 standard [50]. These files were utilised to orient the model for the building process and mathematical slicing, which allowed for layer-by-layer printing by the FDM machine. Following this, the 3D model was converted into printing instruction code (G-code) using the ideaMaker slicer programme. This software featured various options for modifying process parameter settings, such as infill type, calculating the tool path, and regulating the heated bed temperature and fan speed. As the influencing printing parameters were selected (Sect. 2.2), therefore, considering the software settings of the 3D printer, the other printing parameters (as listed in Table 3) for the operation of the 3D printing instrument were kept constant during the printing operation. In this study, a rectilinear infill structure was selected because it presents a high yield on mechanical properties and its ability to provide strong support for solid layers with varying bottom and top thicknesses compared to other infill structures such as honeycomb and triangular [33]. The sliced 3D model was then transferred to an FDM 3D printer through its USB or SD card connector. To ensure printing accuracy and precision, and to provide a better possibility of

Table 3 Fixed printing parameters and their corresponding values

Parameter	Specific parameter	Values (constant)
Layer	Shell thickness	2 mm
	First layer height	0.25 mm
	First layer flowrate	100%
	First layer solid fill pattern type	Lines
Extruder	Extrusion width	0.4 mm
	Retraction speed	40 mm/s
Infill	Infill pattern	Rectilinear
	Infill angle	−45°/45°
	Infill flowrate	100%
	Infill overlap	15%
Solid fill	Bottom solid fill layers	5
	Top solid fill layers	5
	Bottom surface solid fill pattern type	Line
	Top surface solid fill pattern type	Line
Speed	Printing speed	50 mm/s
	Infill speed	50 mm/s
Support	Support structure	None
	Platform addition	Brim
Temperature	Heat bed temperature	45 ℃

Table 2 Experimental layout based on Taguchi L9 OA design

Experimental run	Coded matrix			Un-coded matrix		
	A	B	C	Layer height (mm)	Infill (%)	Nozzle temperature (℃)
1	1	1	1	0.1	60	195
2	1	2	2	0.1	80	205
3	1	3	3	0.1	100	215
4	2	1	2	0.2	60	205
5	2	2	3	0.2	80	215
6	2	3	1	0.2	100	195
7	3	1	3	0.3	60	215
8	3	2	1	0.3	80	195
9	3	3	2	0.3	100	205

predicting the effects of parameters [30], all samples were printed horizontally on the platform, aligned with the print head axis, whilst the vertical orientation was determined by the sample thickness. Prior to conducting every experiment, the build plate was cleaned to ensure that it was free from adhesives and that the process was unaffected [51].

2.5 Characterisation of 3D-printed specimens

Following the 3D printing operation, all samples were kept in a sealed packet, and silica gel was used to avoid moisture absorption. For all the printed samples, tests were carried out at room temperature (typically 23 °C) according to the ASTM-D618-21 [52] standard. The mechanical properties and microstructural testing procedures followed have been described below.

2.5.1 Determination of hardness and surface roughness

The hardness of a material is a fundamental attribute that signifies its ability to withstand localised deformations, such as penetration or indentation on its surface. [53]. The hardness of the printed specimens was assessed using a specialised shore D hardness testing device (Sauter HBD 100–0) that is designed to test the hardness of rigid plastics, thermoplastics, and hard rubber materials. The ASTM-D2240-15 [54] standard, which is commonly employed for assessing the durometer hardness of polymers, was employed as the metric in this test. According to this standard, the thickness of the test specimen should be at least 6.0 mm (0.24 in). Therefore, the dimensions of the hardness test specimens were manufactured with a thickness greater than 6 mm (40mm × 40mm × 8mm), as illustrated in Fig. 2. Five pieces of 3D printed test block were prepared for each experimental condition in an orthogonal array. Nine different surface hardness measurements with 5 mm spaces between each point were collected from each test specimen, resulting in a total of 45 hardness measurements for each experimental run.

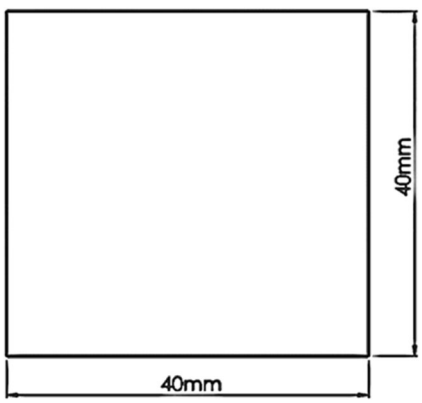

Fig. 2 Schematic diagram of the hardness test specimen

Surface roughness (SR) is utilised as a technical criterion for mechanical components to quantify the existence of micro-irregularities on the surface texture [55]. This property is commonly employed as a technical specification for mechanical products because of its impact on aesthetic appearance and critical role in ensuring the structural precision of a component [56]. In order to evaluate the influence of printing parameters on surface roughness, a Mitutoyo surface roughness tester (model SJ-210) was utilised in this study. This compact and portable device offers a maximum resolution of 0.001 µm. The stylus moves over the sample surface at a predetermined measuring velocity and distance in order to identify any irregularities present on the surface of the workpiece [57]. Roughness was measured on the largest surface of the tensile specimens (Fig. 3). The arithmetic mean roughness (R_a) and root mean square roughness (R_q) were quantitatively measured at the micro-metre (µm) level.

The parameter R_a represents the mean absolute deviation of roughness irregularities from the mean line over a certain length of sampling [58]. The numerical representation of the arithmetic average height parameter is shown by Eq. 1 [58]:

$$R_a = \frac{1}{n}\sum_{i=1}^{n}|y_i| \tag{1}$$

where n represents the total number of samples and y_i represents the deviation from the sample mean line.

The root mean square roughness (R_q) is another significant parameter for characterising surface roughness, which indicates the standard deviation of the distribution of surface heights. The digital representation of this parameter can be mathematically expressed using Eq. 2 [58]:

$$R_q = \sqrt{\frac{1}{n}\sum_{i=1}^{n}|y_i|} \tag{2}$$

where n represents the total number of samples and y_i represents the deviation from the sample mean line.

Since waviness, peaks, and valleys affect the surface quality, five points were chosen on the top side of the tensile specimen to analyse the surface texture with a measuring speed of 0.5 mm/s (Fig. 3), and their mean values were tabulated [59, 60]. Five samples printed from each experimental run were analysed using a tracing length of 5.6 mm, an evaluation length

Fig. 3 Five-point selections from the top surface for surface roughness measurements

of 4.0 mm, and a cut-off wavelength of 0.8 mm to achieve high accuracy and precision, according to ASTM-D7127-17 [61] [59]. The roughness of the printed surface was determined vertically to the feed mark [62]. The representative value of each specimen was determined by calculating the arithmetic mean of five measurements.

2.5.2 Determination of mechanical properties

The mechanical properties of the printed parts were obtained from the tensile, three-point bending (flexural), and impact tests. Following ASTM standards, the standard number of isotropic test specimens per sample was a minimum of five. Hence, for all three tests, five samples were printed for each experimental run. Therefore, 45 specimens were printed for each material (vPLA and rPLA), and in total, 90 specimens were printed for each type of mechanical test (tensile, three-point bending, and impact). The average data were reported based on the testing results of at least five samples for each material batch, along with the calculated standard deviations to evaluate the test reproducibility.

Tensile tests were conducted using dog-bone samples that were fabricated following the ASTM-D638-22 [50] Type IV specifications, with dimensions of 115mm × 19mm × 3.2mm (as shown in Fig. 4). All tests were performed using a Shimadzu Autograph AGS-X tensile testing machine equipped with a 50 kN load cell capacity. This model has an exceptionally high level of precision, with a measurement accuracy within ± 0.5% of the indicated test force. Prior to testing the sample with the instrument, the non-shift wedge-type grips were adjusted to a range of 0 to 7 mm and calibrated according to the ASTM-E4 [63] standard. This instrument uses TRAPEZIUM-X software to manage the test process and thereby pre-process the data acquired from this machine. For the testing operation, at first, sample data such as thickness (mm), breadth (mm), and gauge length (mm) were entered into the software programme. After that, the samples were clamped in the machine and loaded at a crosshead speed of 5 mm/min until failure occurred. The computer software was used to record the force and displacement values. These values were used to generate force–displacement curves using Microsoft Excel, and the ultimate tensile strength (UTS) was evaluated from these data. The elastic modulus of each specimen was evaluated according to the initial slope of its stress/strain curve using Microsoft Excel's 'Trend Line' function. For this purpose, a line diagram was plotted using strain values within the $0.0005 < \varepsilon < 0.0025$ range. Several standard mechanical property evaluations were conducted, including the yield strength, ultimate tensile strength (UTS), work at UTS, and work at fracture, and the average results were tabulated to obtain the arithmetic mean.

The flexural strength (3-point bending) refers to the ability of a material to resist bending forces that act perpendicular to its longitudinal axis. The 3-point bending test specimens (strip-like samples) having dimensions of 127mm × 12.7mm × 3.2mm (as shown in Fig. 5) were prepared and manufactured according to ASTM-D790-17 [64] standard. This test was conducted using Shimadzu Autograph AGS-X equipment with a 10 kN cell mounted with a 3-point bending apparatus, and a displacement rate of 3 mm/min and a span of 51.2 mm (span to depth ratio 16:1) were employed for the test. The instantaneous data for the load and displacement were obtained using the Trapezium-X software.

In this study, the flexural strength was determined by calculating the nominal stress in the central span, which was obtained using the maximum load value, according to Eq. 3 [64],

$$\sigma = \frac{3PL}{2bd^2} \tag{3}$$

where P is the load at a given point on the load–deflection curve, L is the support span length, b is the width, and d is the thickness of the specimen.

The flexural modulus was determined using Eq. 4, as specified in the ASTM-D790-17 [64] standard. This equation was derived through linear regression analysis of the load–displacement curves, considering the linear segment within the range where the correlation coefficient exceeded 95%.

$$E = \frac{L^3 m}{4bd^3} \tag{4}$$

where m represents the slope of the tangent line to the initial linear segment of the load–deflection curve.

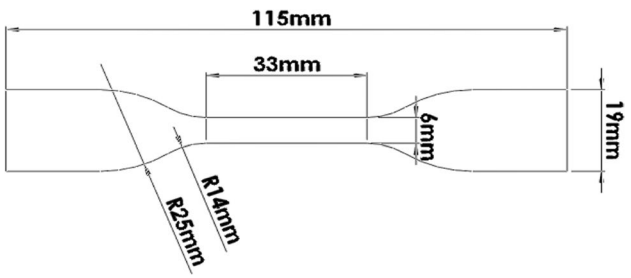

Fig. 4 Schematic diagram of the tensile test specimen

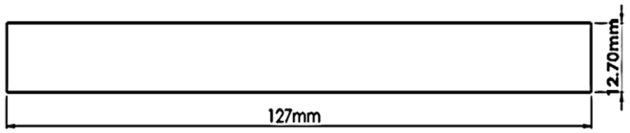

Fig. 5 Schematic diagram of the flexural test specimen

The Charpy impact test, alternatively referred to as the Charpy V-notch test, is a universally accepted method for evaluating the fracture behaviour of materials under high strain rates. This indicates the amount of energy absorbed by the material during the fracture [65]. Charpy impact tests were conducted to evaluate the fracture behaviour of the rPLA-printed specimens. The test specimens were manufactured using dimensions of 127 mm × 12.7 mm × 6.2 mm being notched at a 45° angle in accordance to the ASTM-D6110-18 [66] standard (Fig. 6). A Zwick 5102 (model D-7900) impact tester with a 6.5 J hammer was used to test the fabricated specimens. The impact strength was determined using the energy required to break the specimen and the depth under the notch of the specimen.

2.5.3 Determination of surface morphology

The surface morphology of polymeric materials is a significant characteristic that is originated from their chemical structure and the methods used in their production. These characteristics directly affect the final surface properties of the workpiece [67]. Optical microscopy inspects samples volumetrically and seeks to provide a preliminary perception of the structural features exhibited by a specimen [68]. The focus of this examination is to assess the surface characteristics in relation to printing quality. To examine the surface morphology of the printed samples after mechanical testing, at first, the samples were cut into sections and then embedded within acrylic resin and powder in self-curing polyacrylic cylinders with a dimension of 2 cm width and 3 cm height to expose a flat 4 × 6 mm window of surface for microstructure observations. The test parts (top surface) were prepared through a sequential polishing process utilising silicon carbide (SiC) paper with grit sizes of P400, P800, P1000, P1200, and P4000. Grit sizes determine the particle count in paper according to the Federation of European Producers of Abrasives (FEPA) system, which is the same as the ISO 6344 standard. SiC paper with a higher 'P' value is distinguished by the presence of smaller particles within the paper [69]. Prior to starting the manual polishing of the specimens, the surface was marked with an ink-felt tip permanent marker. The polishing process was performed until the ink was completely removed from the surface, indicating that the current grit size had replaced the previous roughness. The final polishing stage commenced with using diamond suspensions of 6 µm, followed by suspensions of 3 µm and 1 µm. Throughout the process, a continuous water flow was maintained. The specimens were adequately cleaned with water prior to use at higher grit levels. This process aided in the removal of any accumulated abrasive dust, which facilitated clear visualisation of the surface. After completion of the polishing process, the specimens were examined under an optical microscope (OM, OLYMPUS BX51M, Japan) equipped with a portable standalone colour camera. The acquired images were captured at 10 × magnifications by using magnifying lenses. For fractographic analysis, a Pro-MicroScan microscope (model DCM 900) equipped with an eyepiece camera manufactured by the Oplenic Corporation, China, was used to examine the fractured cross-sectional structure of the mechanically tested samples. This examination was primarily concerned with assessing the surface properties associated with the printing quality. A few scratches and voids were observed in the worn area, which may be due to sliding during mechanical property testing.

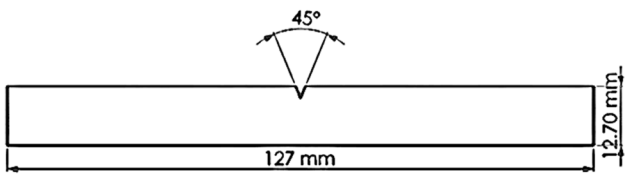

Fig. 6 Schematic diagram of the Charpy impact test specimen

2.6 Assessment using the signal-to-noise ratio

Performance characteristics are fundamental quality features that determine a product's ability to meet specified design requirements. Thus, a product of superior quality will exhibit consistent performance over its entire lifespan and under various operating conditions [70]. The Taguchi method employs a loss function to quantify the difference between the observed and desired values of the performance characteristics, which minimises performance variability. This outcome is then converted into a statistical metric called the signal-to-noise ratio (S/N) ratio to determine the optimal level for each control factor and assess the statistical significance of their impact on the response variable, in other words, to measure the process variability [10, 47]. The term 'noise' refers to the impact of each factor on each operation, whilst the term 'signal' denotes the response to changes in each operating variable [71].

The *S/N* ratio is a metric that considers both the average value and variability of a given quality feature. The specific formula for calculating the *S/N* ratio depends on the criteria used to assess the quality features that need to be investigated [48]. As a consequence, when the process is optimised in terms of *S/N* ratio, it ensures that the resulting optimal process conditions are robust and stable, indicating minimal process variation [72]. Hence, the *S/N* ratio was employed in the current analysis to determine the most favourable and optimal process conditions for the layer height, infill density, and nozzle temperature. The study of the performance characteristics involves the utilisation of three distinct types of *S/N* ratio loss functions: larger-the-better, nominal-the-best,

and smaller-the-better. In the context of smaller-the-better conditions, these characteristics typically represent unfavourable outputs. In contrast, for the larger-the-better condition, the characteristics are generally favourable [73].

2.6.1 Processing of data for S/N value

At first, all output performance responses (data from the experiment) were analysed according to the Taguchi L9 orthogonal array-based design. In this study, the 'larger the better' and 'smaller the better' type S/N ratio responses were used to evaluate the properties of the printed specimens through the FDM process.

This study focuses on maximising the mechanical properties, including tensile strength, three-point bending, impact strength, and hardness. Therefore, the criterion 'larger-the-better' was chosen for these quality characteristics. The principle of 'larger-the-better' was employed in situations where the purpose was to maximise the values of quality characteristics [74]. The larger-the-better S/N ratio was calculated by employing Eq. 5 [75].

$$\frac{S}{N}\text{ratio} = (-10) \times \log_{10}\left(\frac{1}{n}\sum_{i=1}^{n}\frac{1}{y_i^2}\right) \tag{5}$$

where n is the number of trials, i is the experiment number, and y_i is the response in each experiment.

The purpose of the smaller-the-better condition is to minimise the assessment of the quality characteristics to the smallest possible value, ideally zero, a target, or ideal value. Therefore, the principle of 'smaller-the-better' was employed to minimise the surface roughness of specimens produced using vPLA and rPLA. The smaller-the-better S/N ratio was computed by Eq. 6 [75].

$$\frac{S}{N}\text{ratio} = (-10) \times \log_{10}\left(\frac{1}{n}\sum_{i=1}^{n}y_i^2\right) \tag{6}$$

where n is the number of trials, i is the experiment number, and y_i is the response in each experiment.

Once the S/N ratios were evaluated, the average S/N ratios of the parameters at specific levels were examined. After that, the parameter exhibiting the largest difference in arithmetic values between its highest mean S/N ratio and its lowest mean S/N ratio was determined to observe the major impact on the outcome [76]. The Taguchi approach states that when the S/N ratio is maximum, process variability is minimal. The greater the S/N ratio value, the better the outcome since it ensures the maximum quality with the least variability [73]. Therefore, the experimental values with the highest mean S/N ratio were considered as the optimal operating values for each parameter. The influence of each process parameter on the *S/N* ratio at different levels for each sample is presented in the results section, based on an orthogonal experimental design. Finally, the influencing parameters were determined from the calculated S/N ratios, response tables, and main effects plots.

2.7 Analysis of variance (ANOVA)

After statistically examining the S/N ratio, an analysis of variance (ANOVA) was performed to determine the accuracy of the predicted model and to investigate which parameter significantly affected the quality characteristics. ANOVA separates the variation in the dataset into two parts: between-group and within-group [77, 78]. Therefore, ANOVA primarily examines the difference between groups in relation to the variation within each group [79]. ANOVA is a statistical method used to optimise process parameters by analysing a set of experimental results and categorising them according to a common variable or parameter, as well as an objective function or response. This analysis offers valuable insights into the relevance of the observed variance as well as the connection between system parameters and their corresponding responses [76]. F-test and p-test were employed in the ANOVA to assess the extent to which each factor contributed to the overall variation [76]. The F-test was used to determine the parameters that exerted a statistically significant impact on the mechanical properties. In addition, the p value estimated the significance of the results or the extent to which a parameter affects the objective function.

2.7.1 Calculation of the F-ratio

F-ratio is applied in statistical analysis to determine the significant impact of process parameters on product characteristics, which leads to a conclusive outcome [78]. A large F-ratio indicates a higher level of variance between groups compared to within groups, thereby enhancing the likelihood of rejecting the null hypothesis, which suggests that all population means are identical. Generally, the higher the F-ratio, the greater the influence of process parameter modification on the performance characteristics [73]. For the case of $F > 4$, it typically indicates that modifications to the design parameters can have a significant influence on the finished product's characteristics [78].

2.7.2 Calculation of p value

In order to determine the statistical significance of the disparity between group means, it is crucial to consider the p value, which is associated with the F-ratio [77]. The p value is a statistical measure that is used instead of critical values to determine the minimum level of significance for rejecting the null hypothesis. A smaller p value indicates a

higher level of support for the alternative hypothesis [80]. The p value is commonly utilised with a threshold of 0.05, which corresponds to a significance level of 5%. For example, in a case where the calculated p value of a test statistic is less than 0.05, it would be appropriate to reject the null hypothesis [80].

2.8 DoE confirmation test

Once the optimal level of the design parameters had been selected, the final step was conducted to predict and verify the improvement of the quality characteristics using the optimal levels of the design parameters. The obtained results could subsequently be compared to the theoretically predicted optimal conditions based on the desired combination of factors and their respective levels [81]. At first, the predicted S/N ratio, which was expected for the optimal combination of parameters, was determined. After computing the predicted S/N ratio, a confirmation experiment was conducted to validate whether the optimal conditions achieved the expected response. In engineering experiments, it is expected that the level of agreement between the predicted values and confirmation results should fall within the range of $\pm$ 5%, indicating a confidence interval of greater than 95% [81]. This comparison evaluated the agreement between the obtained and expected parameters.

2.9 Statistical analysis

Microsoft Excel (Microsoft Corporation) was used for data handling. Values obtained from the material property characterisation tests are presented as mean $\pm$ standard deviation. Minitab 21 software was used to analyse the *S/N* ratio and ANOVA.

3 Result and discussion

The primary objective of the present investigation was to examine the most favourable printing parameters for the fabrication of 3D printed components utilising two different materials, namely, vPLA and rPLA. The present study employed a Taguchi orthogonal array experimental design to conduct the experiments. The specimens were manufactured using a fused deposition modelling 3D printer. Following the manufacturing process, a comprehensive evaluation of mechanical properties was conducted. The properties under investigation included surface roughness, hardness, tensile strength, flexural strength, and impact strength. The performance of the rPLA specimens was compared/benchmarked with 3D printed vPLA specimens using the same processing parameters. These parameters were carefully assessed to gain insights into the performance characteristics of the printed specimens. In this section, a comprehensive analysis of the results obtained from the experimental testing of the specimens has been presented with the aim of evaluating their material properties.

3.1 Surface roughness

To gain additional insight into the differences between the printed virgin and recycled materials, an analysis of the surface roughness was conducted following printing (as shown in Fig. 7). The FDM process typically results in a relatively rough surface, with the extent of this roughness being influenced by the printing quality [82]. In order to achieve a high level of surface smoothness, it is common practise to subject a product to different processing procedures [3]. Therefore, the experiment aimed to achieve maximum surface smoothness and determine whether the printing parameters under investigation have an impact on the surface roughness of the specimens.

The measurement and recording of the surface roughness for each printed part have been documented in Fig. 7. The findings presented in Fig. 7 (a) indicate that the parameter settings used in experimental run 2 (LH 0.1 mm, I 100%, and NT 205 ℃) yielded the lowest average R_a values for both vPLA and rPLA specimens, namely, 5.87 µm and 6.12 µm, respectively. This was followed by experimental run 3, which resulted in an average R_a value of 6.22 µm and 7.33 µm, and experimental run 3, which yielded average R_a values of 6.70 µm and 7.72 µm, for vPLA and rPLA, respectively. The rPLA specimens exhibited higher R_a and R_q values in comparison to the vPLA specimens, suggesting the presence of rougher surfaces. As recycled PLA is known to exhibit a lower molecular weight due to chain scission, the recycled material would be expected to exhibit a lower viscosity at the same extrusion temperature, leading to the formation of a surface with increased roughness [62]. Based on the data presented in Fig. 7, it can be observed that there is a positive correlation between the nozzle temperature and layer thickness with the surface roughness for both types of materials. Specifically, at a lower nozzle temperature (195 °C) and higher nozzle temperature (215 °C), the surface roughness exhibits an increase. The surface was roughest at 195 °C and slightly less rough at 215 °C, whereas at 205 °C, the surface roughness was lower. Maidin et al. [62] and Mani et al. [83] observed that for vPLA, the surface roughness decreased with an increase in nozzle temperature. It should be noted that the present study used different nozzle temperatures and layer thicknesses, which showed a different result but a similar trend, as in previous research on surface roughness. This may be attributed to the temperature of the nozzle, which significantly affects the raw material melting process. Incomplete melting due to lower than optimum temperature would produce a rough surface.

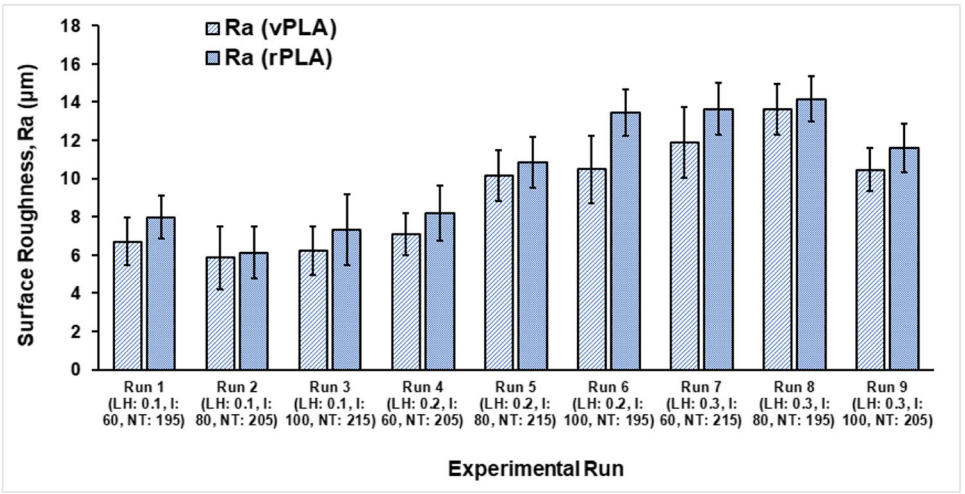

Fig. 7 Surface roughness properties for the vPLA and rPLA printed specimens: **a** R_a and **b** R_q. *LH, layer height; I, infill percentage; NT, nozzle temperature

On the other hand, the reduction in the thickness of the layers has a direct impact on the surface roughness, resulting in decreased visibility of the layers and a smoother surface texture for the printed object. Ayrilmis [84] also observed an increased roughness with increasing printing layer thickness. As the thickness of the layers increases, the surface of the printed part exhibits enhanced sharpness, thereby rendering the individual layers more noticeable [85].

3.2 Hardness test

The hardness test is a widely employed method in the field of plastics to assess the ability of a material to withstand concentrated loads that result in significant plastic deformation. This test is both rigorous and informative and provides valuable insights into the properties of the material under inspection [86]. The findings of the experiments conducted on both materials have been summarised in Fig. 8. The vPLA-printed specimens exhibited marginally higher hardness, whereas the rPLA polymers exhibited lower hardness. The highest shore D hardness was observed for experimental run 9, which indicated hardness result of 81.68 and 76.78 for vPLA and rPLA, respectively. In contrast to this, the lowest result was obtained for experimental run 1, which showed hardness of 79.53 and 73.92 for vPLA and rPLA, respectively. The findings of this study demonstrate a clear positive correlation between nozzle temperature and infill percentage and the resulting increase in hardness, which is consistent with the results evaluated by Mani et al. [83] and Maguluri et al. [87] for vPLA. According to Şirin et al. [88], an increase in the infill percentage resulted in a reduction in void formation, leading to an overall increase in hardness. Another reason is that an increase in the infill percentage leads to an expansion in the cross-sectional area of the material, thereby contributing to the development of a more rigid internal structure [89]. The results also demonstrated the influence of printing temperature on the hardness properties. A reduction in the printing temperature led to a corresponding decrease in the hardness value, the cause of which was attributed to poor layer-to-layer bonding and insufficient melting when printing at low temperatures, which resulted in increased porosity and decreased hardness. The decrease

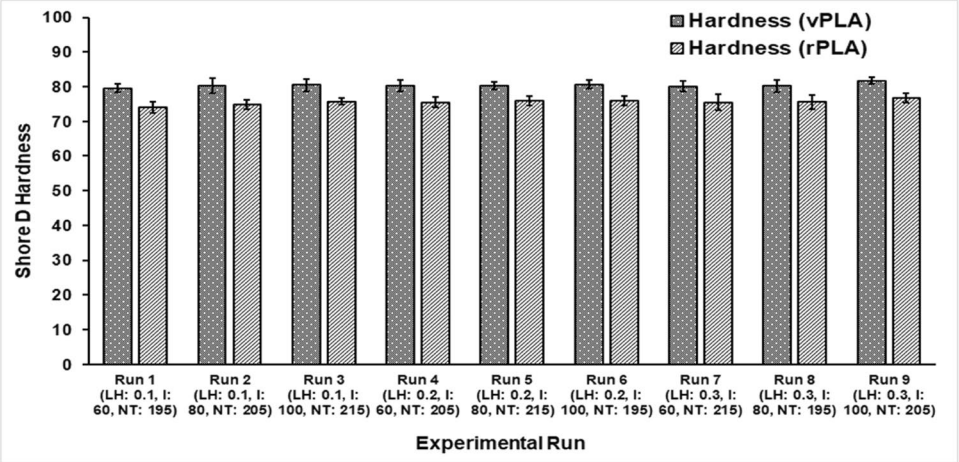

Fig. 8 Shore D hardness values for the vPLA and rPLA specimens. *LH, layer height; I, infill percentage; NT, nozzle temperature

in the rate of hardness change with increasing printing temperature was attributed to the elevated temperature during the printing process and the enhanced adhesion between the fibres, resulting in a more robust material combination. Additionally, a reduction in the number of air gaps can also contribute to this phenomenon [87].

3.3 Tensile test

The output variables of elastic modulus, ultimate tensile strength, yield strength, fracture strength, work at ultimate tensile strength, and work at fracture have been observed by adjusting the input processing variables, as indicated in Table 2. Five specimens were produced for each Taguchi experiment and were chosen for tensile examination to reduce the impact of differences in the specimens on the results of the experiment. The findings from these five specimens demonstrated a consistent level of repeatability. Hence, a single stress–strain curve is illustrated, representing a set of five specimens. Figures 9 and 10 illustrate the stress–strain curves of vPLA and rPLA components manufactured through 3D printing, which included all experimental conditions. It is evident that the vPLA material exhibited higher values of tensile strength and yield strength in comparison to rPLA. The stress–strain relationships exhibited by the vPLA and rPLA specimens demonstrated a nearly linear correlation as the strain increased. Once the stress reached its maximum point, it remained relatively constant as the strain continued to rise. The examination of the outcomes revealed that both the vPLA and rPLA specimens exhibited ductile fracture behaviour. The data clearly indicate that the virgin PLA material exhibited a higher tensile strength than the recycled PLA material.

Tables 4 and 5 summarise the average values of the vPLA and rPLA tensile properties, including the elastic modulus, ultimate tensile strength, yield strength, fracture strength, and strain at fracture, for each specimen designed by the Taguchi method. The results showed that the standard deviation of all the measurements was relatively small, indicating good repeatability within the experimental data. When comparing

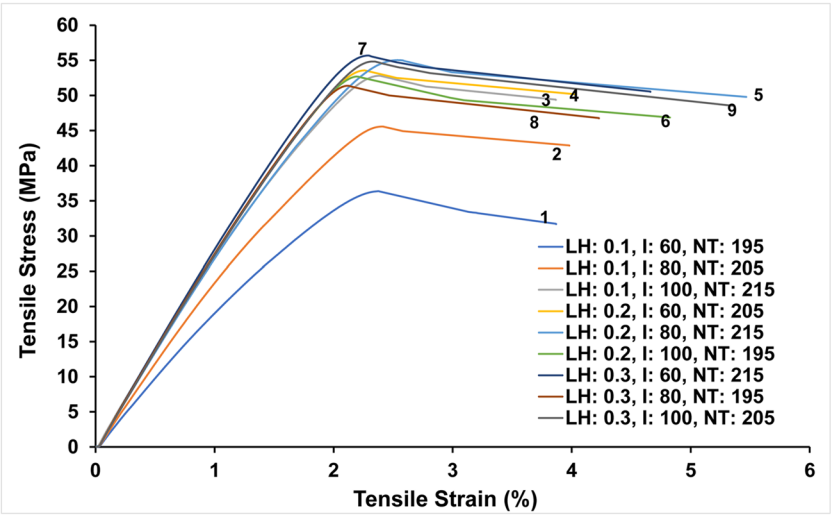

Fig. 9 Tensile stress vs. tensile strain curves for vPLA printed specimens. *LH, layer height; I, infill percentage; NT, nozzle temperature

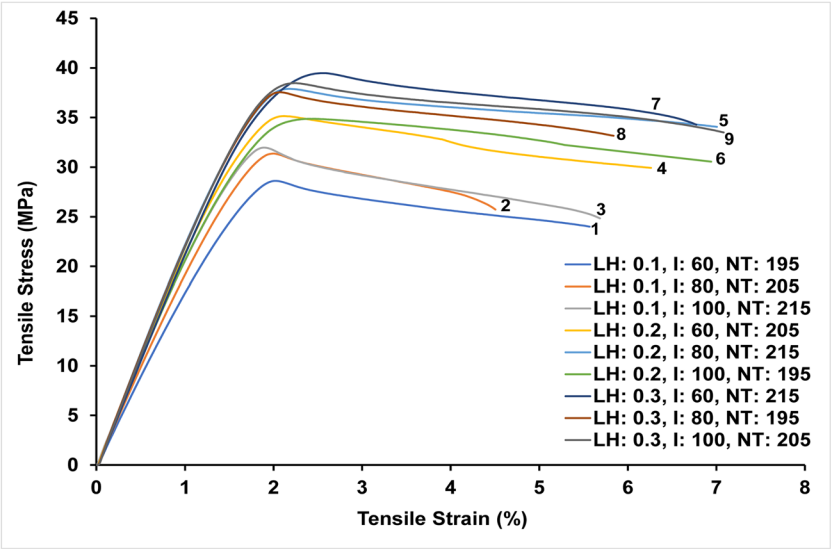

Fig. 10 Tensile stress vs. tensile strain curves for rPLA printed specimens. *LH, layer height; I, infill percentage; NT, nozzle temperature

Table 4 Tensile properties of the vPLA printed specimens

Experimental run	Yield strength (MPa)	Ultimate tensile strength (UTS) (MPa)	Strain at UTS (%)	Fracture strength (MPa)	Strain at fracture (%)	Elastic modulus (GPa)	Work until UTS (kJ/m^2)	Work until fracture (kJ/m^2)
Run 1 (LH 0.1, I 60, NT 195)	33.51 ± 0.871	36.36 ± 0.289	2.27 ± 0.047	31.87 ± 0.619	3.78 ± 0.266	2.26 ± 0.296	32.08 ± 0.770	65.07 ± 1.412
Run 2 (LH 0.1, I 80, NT 205)	38.12 ± 0.931	45.30 ± 0.328	2.48 ± 0.025	42.98 ± 0.389	3.84 ± 0.229	2.71 ± 0.042	40.34 ± 0.340	85.32 ± 0.995
Run 3 (LH 0.1, I 100, NT 215)	47.97 ± 0.954	52.81 ± 0.630	2.50 ± 0.082	49.37 ± 0.829	3.70 ± 0.696	3.13 ± 0.053	43.52 ± 0.944	100.02 ± 1.607
Run 4 (LH 0.2, I 60, NT 205)	50.17 ± 1.124	53.47 ± 0.710	2.49 ± 0.066	50.53 ± 0.951	4.05 ± 0.167	3.10 ± 0.072	43.11 ± 0.632	102.04 ± 0.890
Run 5 (LH 0.2, I 80, NT 215)	50.89 ± 0.991	54.04 ± 0.429	2.51 ± 0.031	51.33 ± 0.659	5.36 ± 0.684	3.11 ± 0.036	47.56 ± 0.871	130.97 ± 1.437
Run 6 (LH 0.2, I 100, NT 195)	48.41 ± 1.202	52.68 ± 0.652	2.41 ± 0.041	47.68 ± 1.012	5.04 ± 0.688	3.08 ± 0.038	42.25 ± 0.205	120.07 ± 2.014
Run 7 (LH 0.3, I 60, NT 215)	53.56 ± 1.141	56.85 ± 0.269	2.48 ± 0.021	52.53 ± 0.475	4.74 ± 0.442	3.19 ± 0.014	45.31 ± 0.537	131.32 ± 1.018
Run 8 (LH 0.3, I 80, NT 195)	50.61 ± 1.123	51.37 ± 0.548	2.37 ± 0.044	50.23 ± 0.613	4.31 ± 0.188	3.04 ± 0.035	41.56 ± 0.759	115.90 ± 1.752
Run 9 (LH 0.3, I 100, NT 205)	51.26 ± 0.984	54.84 ± 0.698	2.45 ± 0.069	51.08 ± 0.286	5.30 ± 0.339	3.10 ± 0.038	46.73 ± 0.409	125.63 ± 1.921

**LH*, layer height; *I*, infill percentage; *NT*, nozzle temperature

the vPLA- and rPLA-printed specimens, it was observed that, in all of the experimental investigations, the vPLA specimens exhibited higher tensile characteristics than the rPLA-printed samples, as depicted in Figs. 9 and 10. In addition, the findings indicated that the samples exhibited better tensile properties as the layer thickness and temperature increased. In previous studies utilising recycled polylactic acid, the same declining pattern in the tensile properties was noted [3, 15, 17, 22, 90].

In the context of experimental run 7, it was observed that specimens printed with a layer height of 0.3 mm, infill density of 80%, and nozzle temperature of 215 °C exhibited the highest tensile strength. This outcome was consistent for both vPLA and rPLA materials. Based on the data presented in Table 4 and 5, it can be observed that the tensile strength of rPLA in experimental run 7 was recorded as 39.90 MPa, which is 25.22% lower than the corresponding value of 56.85 MPa for the vPLA printed specimen. The experimental results indicated that the second highest recorded value was 54.84 MPa for experimental run 9, which utilised a layer height of 0.3 mm, 100% infill, and a nozzle temperature of 205 °C. Similarly, the third highest recorded value was 54.04 MPa for experimental run 5, which employed a layer height of 0.2 mm, 100% infill, and nozzle temperature of 215 °C. In the case of the rPLA-printed specimens, the reduction in the values was 28.85% and 29.09% for the respective parameters. Conversely, a decrease in the thickness of each layer and temperature corresponded to a decline in the tensile strength. To provide an example, the results obtained from experimental run 1 revealed suboptimal results, with vPLA and rPLA demonstrating tensile strength values of 36.06 MPa and 28.81 MPa, respectively.

Table 5 Tensile properties of the rPLA printed specimens

Experimental run	Yield strength (MPa)	Ultimate tensile strength (UTS) (MPa)	Strain at UTS (%)	Fracture strength (MPa)	Strain at fracture (%)	Elastic modulus (GPa)	Work until UTS (kJ/m^2)	Work until fracture (kJ/m^2)
Run 1 (LH 0.1, I 60, NT 195)	22.78 ± 0.442	28.81 ± 0.227	2.06 ± 0.053	23.84 ± 0.919	5.65 ± 0.558	1.99 ± 0.031	26.77 ± 0.682	87.34 ± 0.53
Run 2 (LH 0.1, I 80, NT 205)	25.02 ± 0.738	31.20 ± 0.116	2.01 ± 0.019	25.77 ± 0.901	4.34 ± 0.230	2.19 ± 0.157	29.98 ± 0.331	74.43 ± 1.27
Run 3 (LH 0.1, I 100, NT 215)	25.84 ± 0.696	32.11 ± 0.509	2.00 ± 0.030	26.41 ± 0.863	5.15 ± 1.001	2.32 ± 0.018	24.48 ± 0.862	97.65 ± 1.75
Run 4 (LH 0.2, I 60, NT 205)	31.01 ± 0.458	35.23 ± 0.450	2.21 ± 0.031	29.93 ± 0.645	6.50 ± 1.796	2.42 ± 0.016	29.37 ± 0.774	109.63 ± 2.10
Run 5 (LH 0.2, I 80, NT 215)	32.80 ± 0.437	38.36 ± 0.429	2.17 ± 0.031	33.84 ± 0.392	6.91 ± 0.361	2.59 ± 0.007	34.63 ± 0.730	135.98 ± 1.89
Run 6 (LH 0.2, I 100, NT 195)	29.34 ± 0.436	35.86 ± 0.563	2.24 ± 0.023	30.54 ± 0.732	6.71 ± 0.792	2.38 ± 0.043	31.89 ± 0.521	120.07 ± 2.28
Run 7 (LH 0.3, I 60, NT 215)	34.12 ± 0.648	39.90 ± 0.479	2.36 ± 0.027	34.56 ± 0.992	7.10 ± 0.769	2.66 ± 0.031	40.44 ± 0.507	142.24 ± 2.29
Run 8 (LH 0.3, I 80, NT 195)	31.65 ± 0.394	37.54 ± 0.636	2.06 ± 0.031	33.16 ± 1.357	5.94 ± 1.271	2.51 ± 0.033	30.74 ± 0.461	120.70 ± 2.20
Run 9 (LH 0.3, I 100, NT 205)	33.25 ± 0.723	38.47 ± 0.338	2.16 ± 0.021	28.42 ± 0.462	6.92 ± 0.558	2.62 ± 0.019	34.66 ± 0.722	136.67 ± 2.49

**LH*, layer height; *I*, infill percentage; *NT*, nozzle temperature

The lower printing temperature resulted in incomplete melting, which in turn produced weak bonding between layers and loss of internal structure, resulting in easily fractured specimens [89].

A noteworthy finding was observed in relation to the strain at fracture, wherein rPLA exhibited a superior outcome compared with vPLA, with increases ranging from 14.64 to 68.83%. This ultimately indicated that rPLA demonstrated a more favourable work of fracture. In the case of both the vPLA and rPLA samples, it was observed that experimental run 7 exhibited better fracture performance, including strain at fracture, fracture strength, and work done until fracture, compared to the remaining samples. Experimental runs 5 and 9 exhibited comparable findings to experimental run 7 in terms of the work done until fracture. It is interesting to observe that both the tensile strength and fracture strain were simultaneously improved as the nozzle temperature increased. This phenomenon can be attributed to the improved bond quality between the layers deposited at the interface [10].

Previous research indicated that reducing the infill density leads to a decrease in the contact and adhesion between layers, resulting in a reduction in the mechanical properties [89]. However, the findings of the present study indicate that the infill density did not have a significant impact when the nozzle temperature and layer thickness were suitably high, as observed in experimental run 7. The rationale behind this phenomenon may lie in the reduction of the number of layers during printing with a higher layer thickness, resulting in a decrease in the distortion effect, consequently leading to an increase in strength. Moreover, an increase in the thickness of each layer facilitates the movement of the partially melted substance within the expanded gaps between the printed lines, consequently leading to a notable enhancement in the structural integrity [91]. An additional factor that could contribute to this phenomenon is the utilisation of a higher printing temperature, which increases the fluidity of the material and subsequently enhances the interfacial bond strength between successive layers. Furthermore, the reduction in interchain interaction and decrease in the number of air gaps would be expected to contribute to an increase in the tensile strength of the material, as demonstrated by Hsueh et al. [89].

3.4 Flexural test

The experimental values of flexural properties have been presented in Table 6 and 7. These tables provide a comprehensive overview of the flexural performances of the tested specimens. In addition, the stress vs. strain diagrams for the flexural tests have been depicted in Figs. 11 and 12 and visually illustrate the relationship between stress and strain, thereby offering valuable insight into the mechanical

Table 6 Test results for vPLA flexural specimens

Experimental run	Yield strength	Flexural strength	Flexural strain	Elastic modulus	Work until flexural strength
	MPa	MPa	%	GPa	kJ/m^2
Run 1 (LH 0.1, I 60, NT 195)	60.25 ± 0.25	64.78 ± 2.21	4.78 ± 0.21	2.31 ± 1.20	28.74 ± 1.41
Run 2 (LH 0.1, I 80, NT 205)	66.44 ± 0.58	71.15 ± 1.21	5.11 ± 0.85	2.56 ± 1.24	31.11 ± 2.20
Run 3 (LH 0.1, I 100, NT 215)	73.85 ± 1.20	79.98 ± 1.48	5.23 ± 0.98	2.94 ± 1.24	35.86 ± 2.01
Run 4 (LH 0.2, I 60, NT 205)	69.45 ± 1.07	82.75 ± 2.01	6.60 ± 0.67	2.91 ± 1.83	39.47 ± 1.91
Run 5 (LH 0.2, I 80, NT 215)	74.11 ± 0.87	87.39 ± 1.24	6.92 ± 0.70	2.91 ± 1.51	40.87 ± 1.01
Run 6 (LH 0.2, I 100, NT 195)	70.72 ± 1.23	82.53 ± 1.09	7.90 ± 1.24	2.89 ± 1.81	45.83 ± 1.46
Run 7 (LH 0.3, I 60, NT 215)	77.34 ± 0.89	92.44 ± 2.01	6.85 ± 1.20	3.01 ± 0.95	49.96 ± 1.47
Run 8 (LH 0.3, I 80, NT 195)	71.48 ± 1.87	86.11 ± 2.42	8.11 ± 0.51	2.85 ± 0.89	46.07 ± 2.03
Run 9 (LH 0.3, I 100, NT 205)	76.60 ± 1.74	90.26 ± 1.74	6.50 ± 0.81	2.95 ± 1.01	46.35 ± 1.58

**LH*, layer height; *I*, infill percentage; *NT*, nozzle temperature

behaviour of the specimens under flexural loading. The flexural stress–strain diagrams were determined using Eqs. 4 and 5, respectively. Work until flexural strength was determined from the area under the bending load–displacement curve until the point of maximum stress. During loading, the fracture strength of the flexural tests could not be determined, because the samples did not completely fracture up to the testing limit. All tests were terminated before the specimens reached their fracture point because they came into contact with the grips prior to fracture. This was primarily attributed to the excessive ductility of the polymers; therefore, the measurement of strain at fracture was not achieved [3, 92]. The findings presented in this study showed comparatively poorer mechanical properties exhibited by the specimens printed using rPLA in comparison to those printed using vPLA. In previous investigations employing rPLA, a comparable finding related to a decreasing trend in flexural characteristics was documented [3, 17, 22]. This phenomenon can be attributed to the reduced mechanical properties of recycled PLA owing to its low molecular weight [93].

According to the findings presented in Table 6 and 7, it is evident that experimental run 7 yielded the highest value for all the flexural properties. Specifically, this condition demonstrated a maximum flexural strength of 92.44 MPa for vPLA and 84.74 MPa for rPLA. This result may be attributed to the fact that experimental run 7 was printed with a high nozzle temperature and high layer height, which resulted in improved layer adhesion and minimal void formation; as a consequence, the specimens exhibited excellent flexural properties in comparison to other conditions [94]. In contrast to this, the findings of experimental run 1 yielded unsatisfactory outcomes for both vPLA and rPLA with respective flexural strengths of 64.78 MPa and 46.78 MPa. The stress and strain curves

Table 7 Test results for rPLA flexural specimens

Experimental run	Yield strength	Flexural strength	Flexural strain	Elastic modulus	Work until flexural strength
	MPa	MPa	%	GPa	kJ/m^2
Run 1 (LH 0.1, I 60, NT 195)	41.50 ± 1.23	46.78 ± 1.83	8.75 ± 2.21	1.86 ± 2.41	71.93 ± 1.10
Run 2 (LH 0.1, I 80, NT 205)	43.15 ± 1.74	52.31 ± 1.94	8.95 ± 2.85	2.05 ± 1.08	73.44 ± 0.95
Run 3 (LH 0.1, I 100, NT 215)	53.02 ± 0.84	65.54 ± 0.89	9.20 ± 1.27	2.13 ± 1.30	79.01 ± 2.01
Run 4 (LH 0.2, I 60, NT 205)	63.40 ± 1.01	75.84 ± 1.38	7.71 ± 1.38	2.35 ± 1.49	84.48 ± 1.28
Run 5 (LH 0.2, I 80, NT 215)	68.35 ± 0.51	82.40 ± 2.01	8.55 ± 1.78	2.40 ± 1.74	92.66 ± 1.87
Run 6 (LH 0.2, I 100, NT 195)	60.33 ± 1.21	74.22 ± 1.89	8.50 ± 2.12	2.19 ± 2.41	82.50 ± 1.91
Run 7 (LH 0.3, I 60, NT 215)	72.06 ± 1.87	84.74 ± 2.24	9.90 ± 1.45	2.52 ± 1.34	93.45 ± 2.41
Run 8 (LH 0.3, I 80, NT 195)	66.34 ± 0.98	79.70 ± 1.56	8.70 ± 1.81	2.36 ± 2.29	85.94 ± 1.01
Run 9 (LH 0.3, I 100, NT 205)	67.33 ± 1.23	81.44 ± 2.03	8.77 ± 1.78	2.48 ± 2.10	86.36 ± 1.58

**LH*, layer height; *I*, infill percentage; *NT*, nozzle temperature

for vPLA (Fig. 11) showed that experimental run 7 possessed maximum strength, but that the strain capacity was not maximum. Experimental run 8 exhibited lower flexural strength in comparison with experimental run 7, but it demonstrated greater ductility because of its better strain-absorbing capacity. This was attributed to the domination of additional porosity within the sample due to the lower melting temperature, which resulted in increased deflection [1]. The stress–strain curves, as illustrated in Fig. 12, provide valuable insights into the mechanical properties of rPLA. Notably, analysis of the stress and strain curves revealed that experimental run 7 exhibited the highest levels of flexural stress and strain amongst all of the samples tested. In comparing the two curves, it became apparent that the strain displayed by rPLA is greater in magnitude when compared to that of vPLA. The rationale behind this phenomenon was that elongation of thermoplastic polymers is directly influenced by the recycling process. As previously mentioned, the thermal degradation process during recycling induces chain scissoring, which subsequently causes a reduction in the strength of the intermolecular bonds within the polymers. Hence, the polymers demonstrated a tendency to undergo elongation [95].

3.5 Impact strength

In relation to the influence of the printing parameters on the impact strength, Fig. 13 presents the average Charpy impact values, which exhibit a direct correlation with the infill percentage and layer thickness. The study conducted by Kamaal et al. [96] found that there was no significant difference in

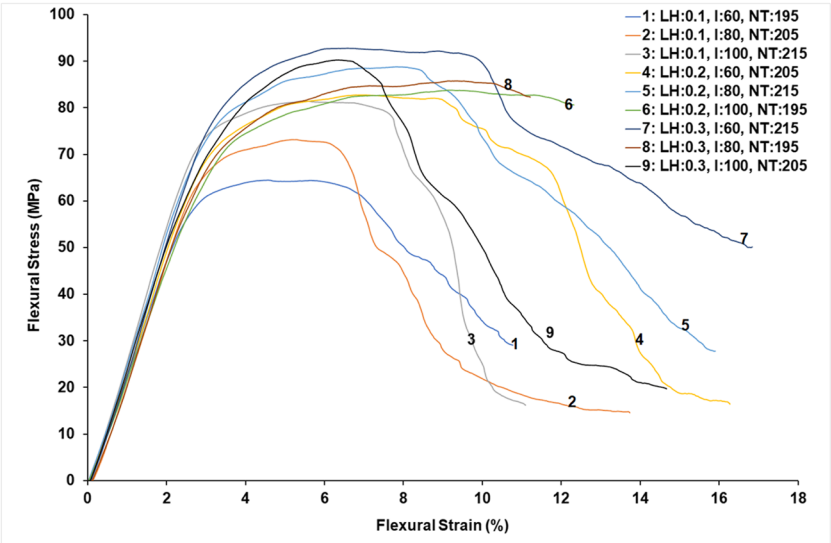

Fig. 11 Flexural stress vs. flexural strain curves for vPLA specimens. *LH, layer height; I, infill percentage; NT, nozzle temperature

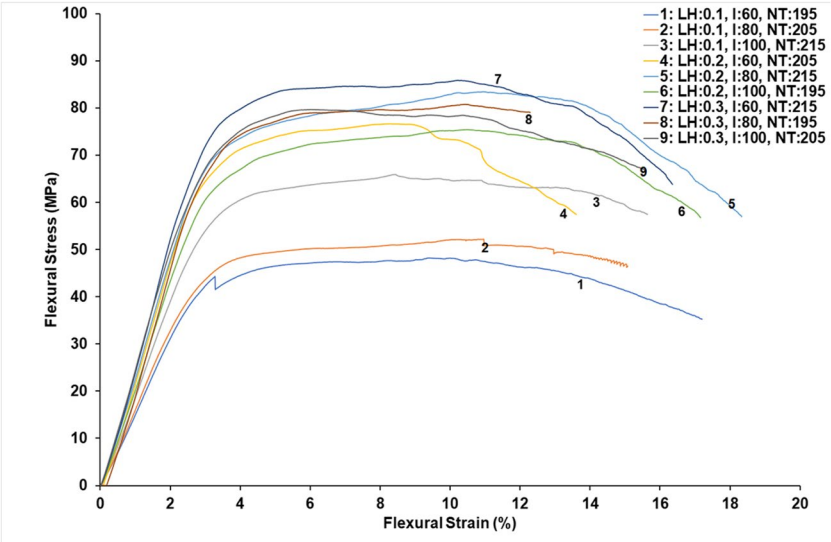

Fig. 12 Flexural stress vs. flexural strain curves for rPLA specimens. *LH, layer height; I, infill percentage; NT, nozzle temperature

impact strength at low infill percentages. However, this study observed that when the infill percentage reached 100%, and the layer height was 0.3 mm, there was an increase in impact strength. This can be attributed to the reduction in voids within the printed material, as well as the increased amount of material available to absorb the impact energy [97]. The outcome of the impact tests indicated that rPLA exhibited an impact strength that is comparable to that of vPLA. The impact strength of the components made from recycled PLA exhibited only a marginally reduced value (ranging from 4.06 to 11.08%) when compared to the components made from virgin PLA. Experimental run 9 exhibited the highest average impact value for both the vPLA and rPLA specimens. In contrast to this, the sample with the lowest average value was observed in experimental run 1 when the layer thickness was reduced, with this being consistent with Atakok et al. [17], who found a decrease in impact strength as the layer height decreased, with this being attributed to the reduced resistance to crack propagation.

3.6 Fractography studies

The experimental tests revealed that the nature of fracture for the vPLA and rPLA specimens was ductile, which was due to stretching and reorientation of the material that resulted in deformation. The fracture surfaces of the 3D printed PLA samples exhibited a ductile type of fracture. The fracture surfaces were analysed using an optical microscope with results being presented in Figs. 14 and 15. It can be seen from Fig. 14 that a large number of pores were present when the layer thickness was low, even though the infill amount and temperature were high (run 1) as shown in Fig. 14a, which resulted in poor bonding of the material. When the layer thickness and nozzle temperature were high (run 7), a smaller number of pores were present, as shown in Fig. 14b, with this being mainly attributed to the increase in partially melted polymer within the expanded gaps between the printed lines, consequently leading to a notable enhancement in structural integrity. However, when the layer thickness and infill were high, but the nozzle temperature was low (run 9), the presence of pores increased compared to run 7, but it was still very small compared to run 1 (shown in Fig. 14c). In contrast to this, it was observed from Fig. 14 that, although the infill and layer thickness increased, if the nozzle temperature was low then the presence of large voids was noted (Fig. 14d). This was attributed to the low fluidity of the material, which ultimately increased the size and quantity of pores. For the case of rPLA, the same type of observations was made. In this case, large voids were observed for the same experimental conditions as had been noted for vPLA, i.e., Fig. 15a–d. An in-depth investigation utilising microscopy tools was conducted to identify the underlying factors contributing to the observed reduction in mechanical strength caused by variations in the nozzle temperature. The findings indicate that the inadequate flow of material, stemming from a lower nozzle temperature during the deposition process, leads to the formation of gaps and voids within the layers. Although the infill density, as specified in the slicing software, was set to 100%, the presence of voids was observed [98]. Figure 16a–c shows that with decreasing nozzle temperature, the voids between layers increased owing to the poor adhesion between layers, which ultimately decreased the strength of the rPLA samples. In conclusion, this analysis showed a positive correlation between layer thickness and nozzle temperature, i.e., even for the same nominal layer thickness, increasing the nozzle temperature led to a larger actual layer thickness. Thus, the nozzle temperature and layer thickness must be selected appropriately to improve the microstructure of the specimen. Overall, a good correlation was noted between the optical microscopic studies and the resulting experimental data.

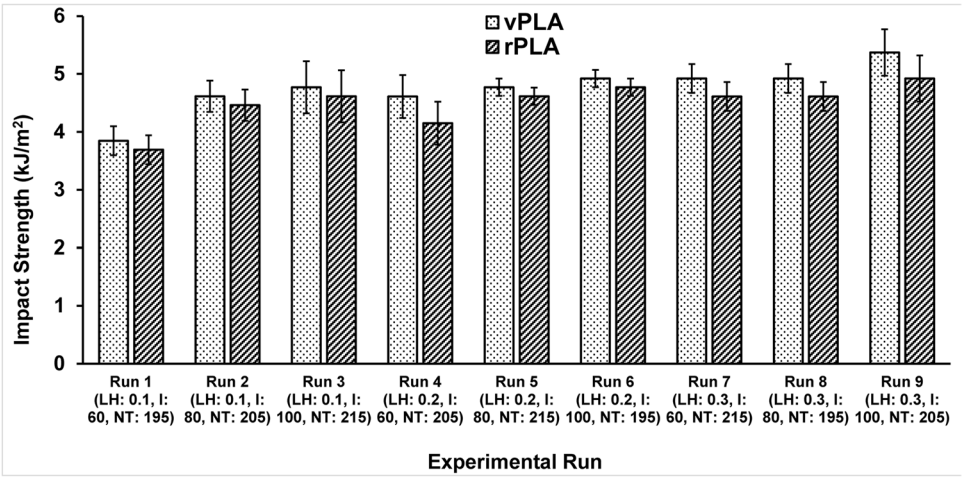

Fig. 13 Impact strength experimental results for vPLA and rPLA specimens. *LH, layer height; I, infill percentage; NT, nozzle temperature

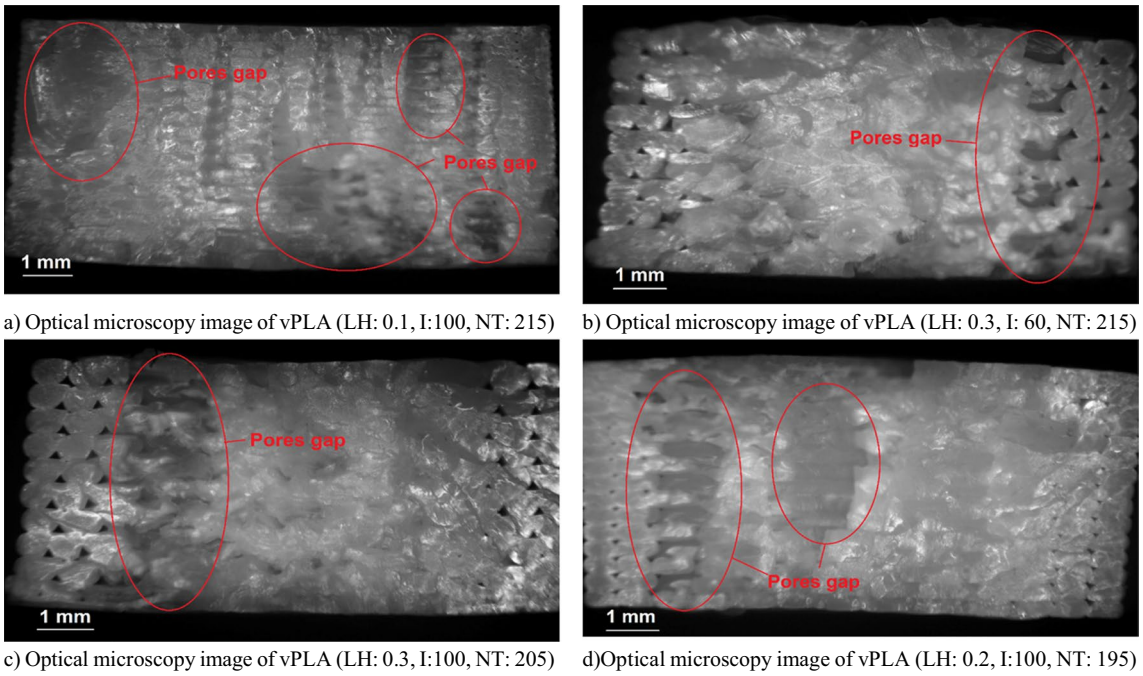

a) Optical microscopy image of vPLA (LH: 0.1, I:100, NT: 215)
b) Optical microscopy image of vPLA (LH: 0.3, I: 60, NT: 215)
c) Optical microscopy image of vPLA (LH: 0.3, I:100, NT: 205)
d)Optical microscopy image of vPLA (LH: 0.2, I:100, NT: 195)

Fig. 14 Optical micrographs of fractured surfaces of vPLA specimens: **a** run 3, **b** run 7, **c** run 9, and **d** run 6

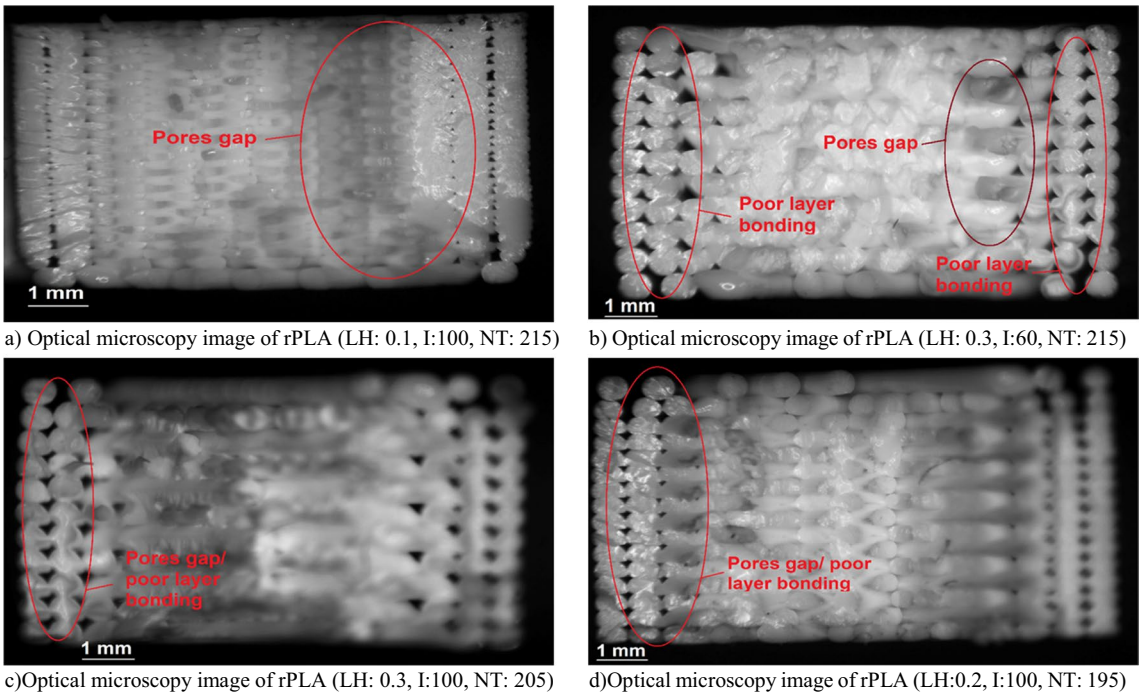

a) Optical microscopy image of rPLA (LH: 0.1, I:100, NT: 215)
b) Optical microscopy image of rPLA (LH: 0.3, I:60, NT: 215)
c)Optical microscopy image of rPLA (LH: 0.3, I:100, NT: 205)
d)Optical microscopy image of rPLA (LH:0.2, I:100, NT: 195)

Fig. 15 Optical micrographs of fracture surfaces for rPLA specimens: **a** run 3, **b** run 7, **c** run 9, and **d** run 6

3.7 Optimisation of process parameters

The optimisation of process parameters within the FDM 3D printer with respect to hardness, tensile strength, and surface roughness was carried out using Taguchi analysis and the Minitab 21 software. The *S/N* ratios for tensile, flexural, impact strength, hardness, and surface roughness were evaluated with 'larger the better' criteria for tensile properties, flexural properties, impact strength and hardness, and 'lower the better' criteria for surface roughness. The optimal levels were determined by utilising the average *S/N* ratios for each response at each level. A higher value of *S/N* ratio indicates superior quality characteristics [23]. Therefore, to maximise the mechanical strength, the optimal parameters were selected by choosing the highest *S/N* ratio for each factor.

Figure 17 shows a comparison of the main effects plot, illustrating the *S/N* ratios for both the vPLA and rPLA tensile properties, as well as the FDM printing parameters. The figure reveals that layer thickness was the most significant factor affecting tensile properties, and the temperature of the nozzle head also had a substantial impact on strain at UTS. It is anticipated that the melt viscosity of PLA is highly influenced by temperature, and as the nozzle temperature increases during the printing process, the melt viscosity of PLA decreases, thereby leading to improved interlayer adhesion [99]. As shown in Fig. 17, the optimum combination of parameters was found to be A3B3C3, with a layer thickness of 0.3 mm, infill of 100%, and a nozzle temperature of 215 °C.

Figure 18 illustrates the *S/N* ratio and main effects plot for flexural strength (FS) for the larger-the-better criteria. The FS exhibited an almost identical parametric response to that of the tensile strength. Here, it was determined that the flexural characteristics exhibited maximum values when the layer thickness, infill density, and nozzle temperature were adjusted to high levels. Therefore, for the maximum flexural strength response, 0.3 mm layer thickness, 100% infill, and 215 °C nozzle temperature were determined to be the optimal combination of parameters. The reasoning behind this combination was the same as already discussed for the case of tensile strength.

From a dynamic application standpoint, maximising the required impact strength would be important [21]. In the current study, the resulting Charpy impact strengths were examined under the condition of larger the better, as illustrated in Fig. 19. Analysis of the S/N ratio response plots

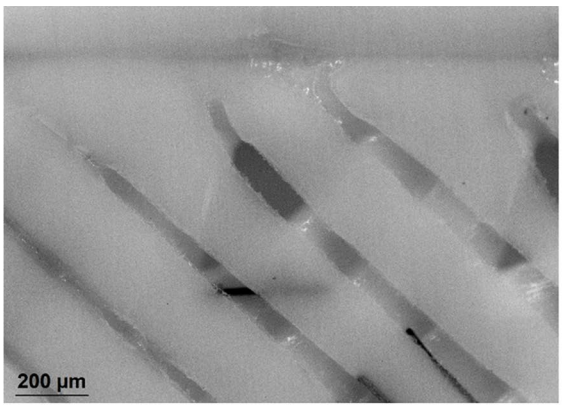

a) Optical microscopy image of rPLA (LH: 0.3, I: 80, NT: 195)

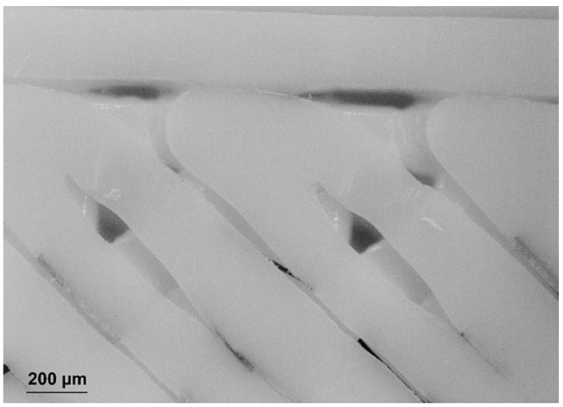

b) Optical microscopy image of rPLA (LH: 0.3, I: 100, NT: 205)

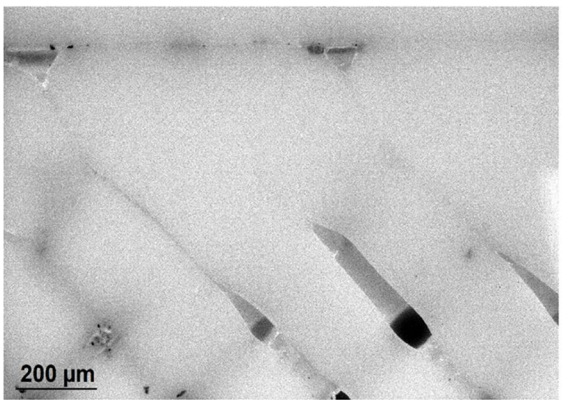

c)Optical microscopy image of rPLA (LH: 0.3, I: 60, NT: 215)

Fig. 16 Micrographs of the cross-sectional area of printed samples: **a** run 8, **b** run 9, and **c** run 7

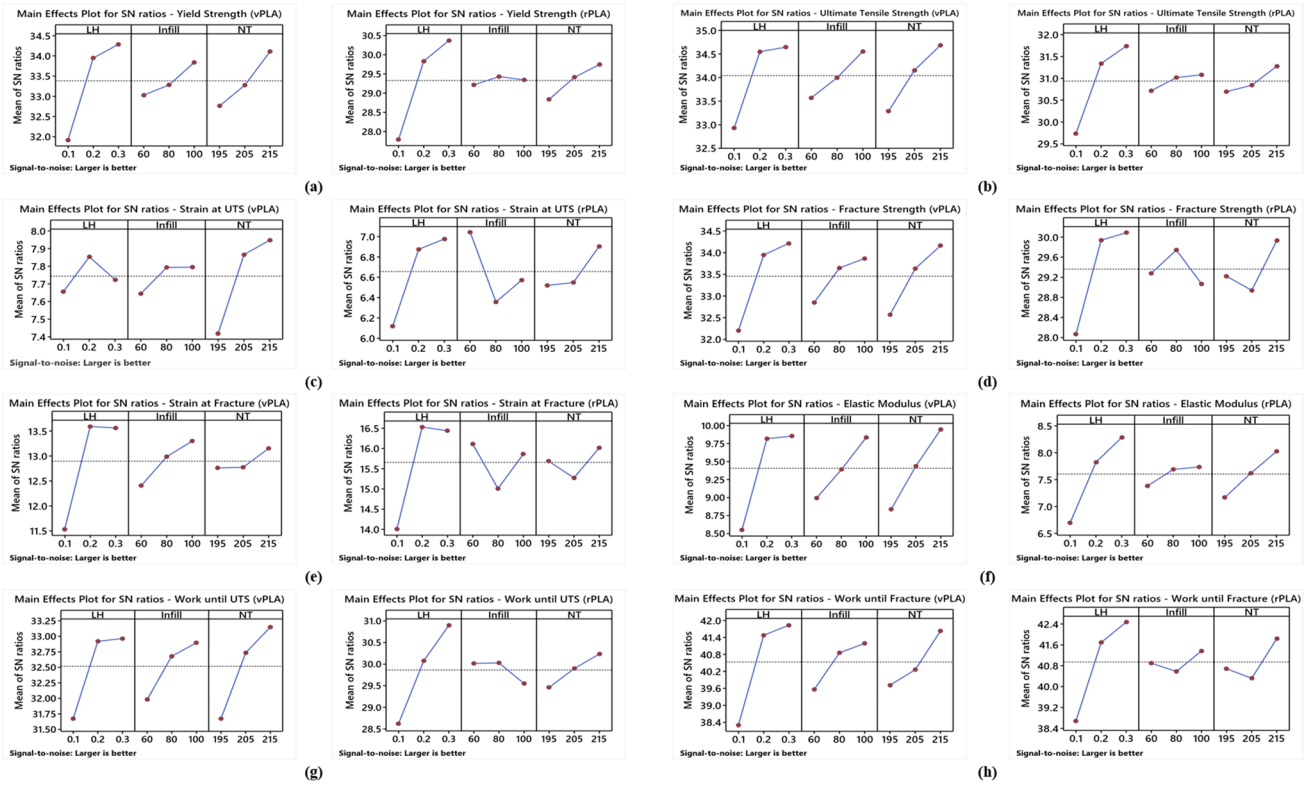

Fig. 17 Main effects plot showing *S/N* ratios for tensile properties of vPLA and rPLA specimens: **a** yield strength, **b** UTS, **c** strain at UTS, **d** fracture strength, **e** strain at fracture, **f** elastic modulus, **g** work until UTS, and **h** work until fracture

revealed that the layer height and infill significantly affected the impact strength of the vPLA and rPLA-printed specimens. However, it was observed that nozzle temperature did not significantly influence the impact properties, such as had been the case for TS and FS. Therefore, 0.3 mm layer thickness, 100% infill, and 205 °C nozzle temperature were determined to be the optimal combination to achieve high impact strength. In particular, the interlayer bonding exhibited poor performance at 195 °C but improved when the temperature was raised to 205 °C. However, a further increase in the temperature resulted in increased fluidity of the molten plastic, leading to a decrease in viscosity and the formation of voids. Consequently, this had a slight negative impact on the overall performance in terms of impact strength [97].

The experimental findings were examined in order to determine the optimal printing parameters for minimising surface roughness. The analysis was conducted based on the *S/N* ratios, employing the 'smaller the better' criteria and presented in Fig. 20. The investigation revealed that the primary factor contributing to the reduction in the surface roughness of the specimens was the reduction in layer height. Furthermore, the main effects plot demonstrated that low density had a statistically significant impact on surface roughness. Therefore, the most favourable arrangement of processing parameters for minimising surface roughness was determined as follows: a layer thickness of 0.1 mm, an infill percentage of 60%, and a nozzle temperature of 205 °C for vPLA; a layer thickness of 0.1 mm, an infill percentage of 60%, and a nozzle temperature of 205 °C for rPLA.

Figure 21 presents the *S/N* ratios and mean plots (using the 'larger the better' criterion) for shore D hardness of the 3D printed specimens. Overall, it was found that the specimen hardness increased by increasing the infill density, layer height, and nozzle temperature for vPLA. The reason behind this trend was ascribed to the reduction in porosity, which would be expected to improve the hardness [21]. However, a layer thickness of 0.2 mm exhibited the highest hardness for rPLA and, therefore, the optimum combinations were found to be layer height of 0.3 mm, infill of 100%, and nozzle temperature of 215 ℃ for vPLA and 0.2 mm layer height, 100% infill, and 215 ℃ nozzle temperature for rPLA.

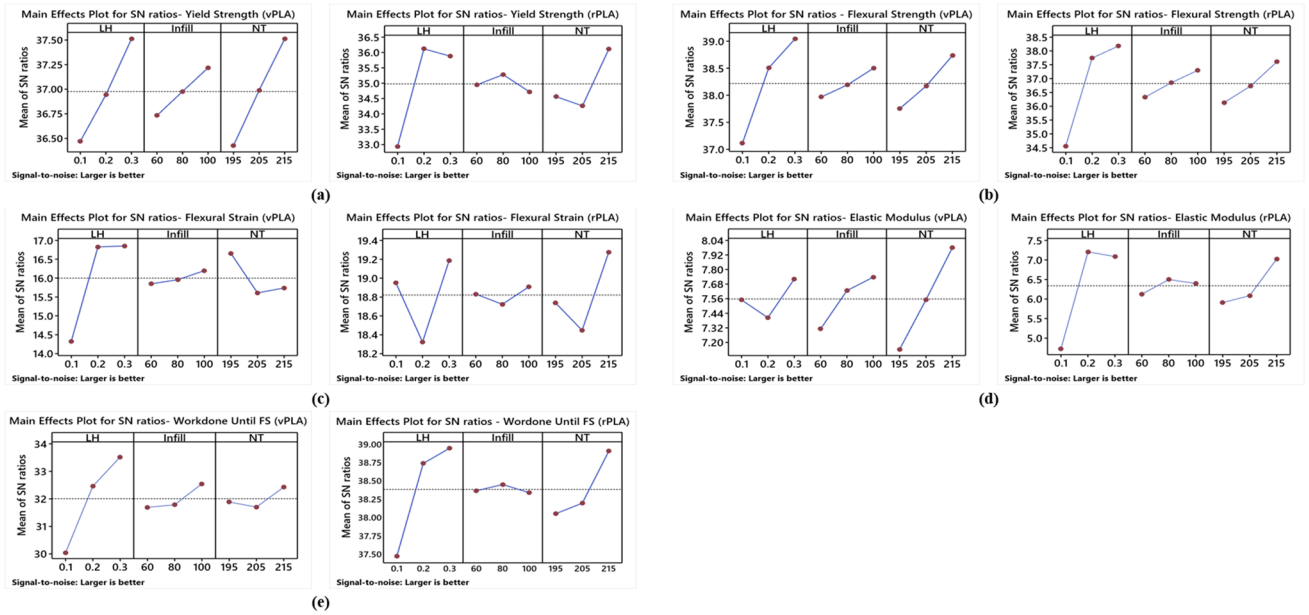

Fig. 18 Main effects plot of *S/N* ratios for flexural properties of vPLA and rPLA specimens: **a** yield strength, **b** flexural strength, **c** flexural strain, **d** elastic modulus, and **e** work until flexural strength

3.8 ANOVA analysis

An ANOVA study was conducted with a confidence level of 95% to examine the relative contribution of the parameters on the individual responses of the tensile strength, flexural strength, impact strength, shore D hardness, and surface roughness properties of both virgin PLA and recycled PLA materials. Table 8 shows the ANOVA results, where the rows labelled as 'Residual Error' refer to the errors that arise from uncontrollable factors, specifically noise, which are not accounted for in the experiment and are thus considered as experimental errors [100]. A low residual error was observed for each property that exhibited good control over the processing of components. The main purpose of the percentage contribution is to assess the extent to which different parameters influence mechanical properties. In other words, a higher percentage value indicates a stronger influence of a particular parameter on the response variable [101]. The findings indicated that the layer thickness had a higher percentage contribution to the parameters examined (as shown in Table 8) compared to the infill and nozzle temperatures. Therefore, the major

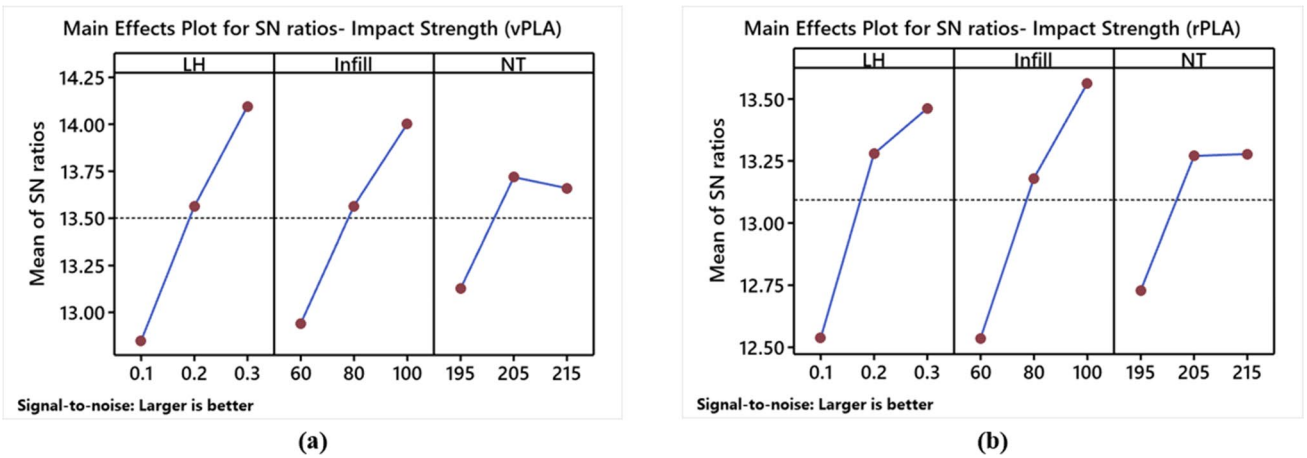

Fig. 19 Main effects plot of *S/N* ratios for impact strengths of **a** vPLA and **b** rPLA specimens

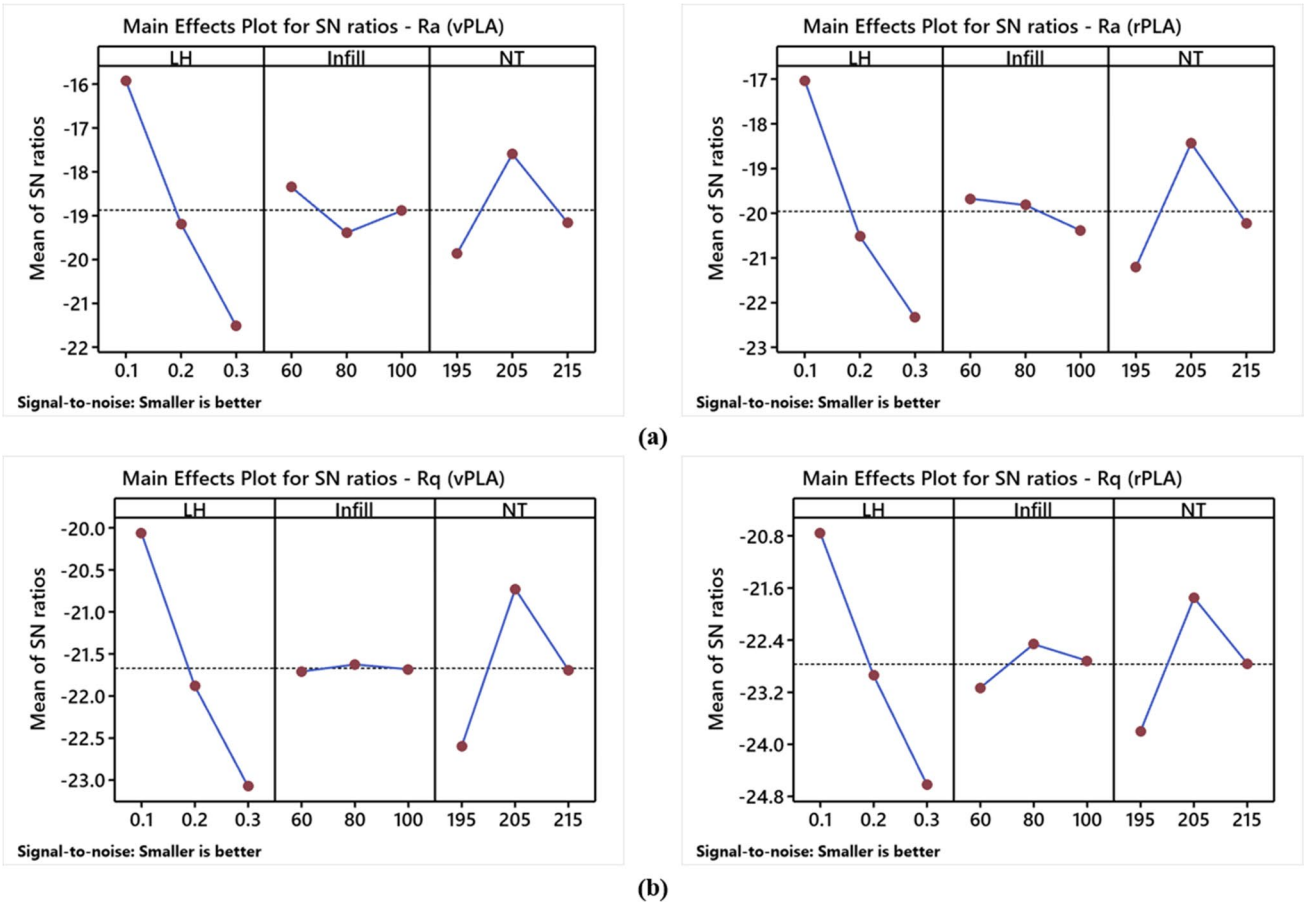

Fig. 20 Main effects plot of *S*/*N* ratios for the surface roughness of vPLA and rPLA specimens: **a** R_a and **b** R_q

determinant for the properties investigated in this work was found to be the layer thickness. The second factor that exerted an influence on the system was the nozzle temperature. In contrast to this, the influence of the infill percentage on the outcome was found to be negligible (at least within the range of 60–100% investigated in this work). From the ANOVA results, it was determined that overall optimum tensile and flexural strength could be achieved by selecting high layer thickness, high nozzle temperature, and low infill density.

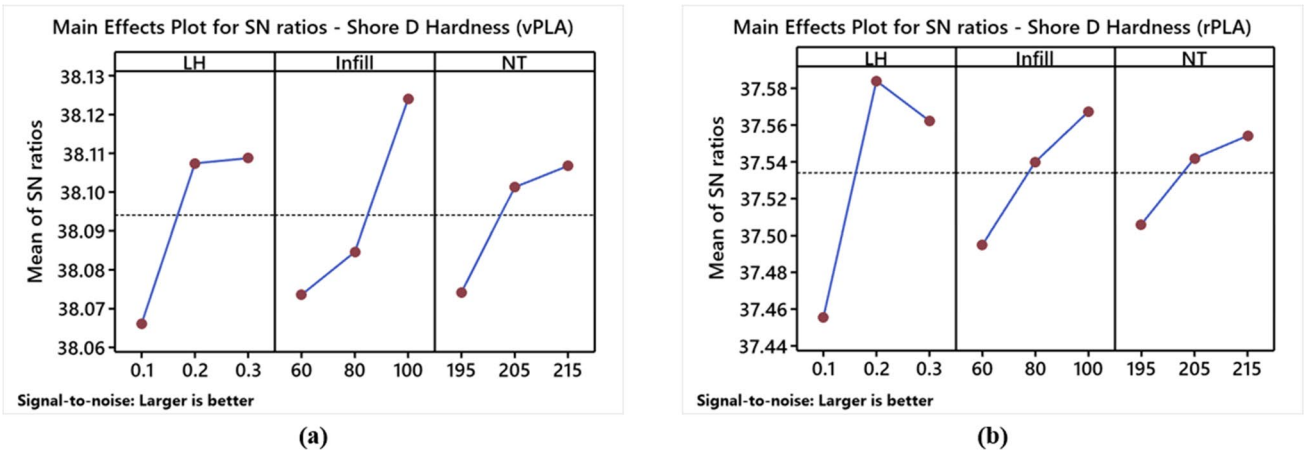

Fig. 21 Main effects plot of *S*/*N* ratios for shore D hardness of (**a**) vPLA and (**b**) rPLA specimens

Table 8 ANOVA responses for *S/N* ratios of various properties examined in this work

Response	Source	DF	Seq SS	Adj SS	Adj MS	*F*	*p*	% contribution
Ultimate tensile strength (vPLA)	LH	2	3.09	3.09	1.54	130.35	0.008	68.04
	Infill	2	0.19	0.19	0.09	8.17	0.109	4.27
	NT	2	1.23	1.23	0.61	52.05	0.019	27.17
	Residual error	2	0.023	0.02	0.01			0.52
	Total	8	4.55					100.00
Ultimate tensile strength (rPLA)	LH	2	2.94	2.94	1.47	273.29	0.004	73.48
	Infill	2	0.14	0.14	0.07	13.04	0.071	3.51
	NT	2	0.91	0.91	0.45	84.58	0.012	22.74
	Residual error	2	0.01	0.01	0.00			0.27
	Total	8	4.01					100.00
Flexural strength (vPLA)	LH	2	5.97	5.97	2.98	39.68	0.025	74.55
	Infill	2	0.43	0.43	0.22	2.86	0.259	5.38
	NT	2	1.46	1.46	0.73	9.68	0.094	18.19
	Residual error	2	0.15	0.15	0.08			1.88
	Total	8	8.00					100.00
Flexural strength (rPLA)	LH	2	23.50	23.50	11.75	23.61	0.041	80.39
	Infill	2	1.42	1.42	0.71	1.43	0.412	4.86
	NT	2	3.31	3.31	1.65	3.33	0.231	11.35
	Residual error	2	0.99	0.99	0.49			3.40
	Total	8	29.23					100.00
Impact strength (vPLA)	LH	2	2.35	2.35	1.17	10.88	0.084	47.72
	Infill	2	1.72	1.72	0.86	7.96	0.112	34.91
	NT	2	0.64	0.64	0.32	2.96	0.252	12.99
	Residual error	2	0.22	0.22	0.11			4.38
	Total	8	4.92					100.00
Impact strength (rPLA)	LH	2	1.44	1.44	0.72	4.16	0.194	35.98
	Infill	2	1.62	1.62	0.81	4.68	0.176	40.50
	NT	2	0.60	0.60	0.30	1.72	0.368	14.86
	Residual error	2	0.35	0.35	0.17			8.65
	Total	8	4.01					100.00
Shore D hardness (vPLA)	LH	2	0.003	0.003	0.001763	2.46	0.289	32.11
	Infill	2	0.004	0.004	0.0021	2.93	0.254	38.24
	NT	2	0.001	0.001	0.000911	1.27	0.44	16.59
	Residual error	2	0.001	0.001	0.000716			13.05
	Total	8	0.011					100.00
Shore D hardness (rPLA)	LH	2	0.028	0.028	0.014	28.77	0.034	68.94
	Infill	2	0.008	0.008	0.004	8.13	0.11	19.49
	NT	2	0.003	0.003	0.001	3.83	0.207	9.17
	Residual error	2	0.001	0.001	0.0004			2.40
	Total	8	0.041					100.00
Surface roughness Ra (vPLA)	LH	2	47.42	47.42	23.71	85.37	0.012	82.09
	Infill	2	1.63	1.63	0.81	2.95	0.253	2.83
	NT	2	8.15	8.15	4.07	14.68	0.064	14.11
	Residual error	2	0.55	0.55	0.27			0.96
	Total	8	57.76					100.00
Surface roughness Ra (rPLA)	LH	2	43.64	43.64	21.82	44.58	0.022	75.99
	Infill	2	0.85	0.85	0.42	0.87	0.536	1.48
	NT	2	11.96	11.96	5.98	12.22	0.076	20.83
	Residual error	2	0.98	0.98	0.49			1.70
	Total	8	57.43					100.00

**DF* represents the degree of freedom; *Seq SS* represents the sequential sum of squares; *Adj SS* represents the adjusted sum of squares; *Adj MS* represents the adjusted mean square; *F* represents the ratio of explained variance to unexplained variance; *p* represents the probability of obtaining *F* value

Table 9 Summary of the optimum parameters required to attain the highest possible mechanical characteristics

Factors	Tensile Strength				Flexural Strength				Impact Strength			
	vPLA		rPLA		vPLA		rPLA		vPLA		rPLA	
	Level	Description	Level	Description	Level	Description	Level	Description	Level	Description	Level	Description
Layer Height (mm)	3	0.3	3	0.3	3	0.3	3	0.3	3	0.3	3	0.3
Infill (%)	3	100	3	100	3	100	3	100	3	100	3	100
Nozzle Temperature (°C)	3	215	3	215	3	215	3	215	2	205	3	215
Factors	Shore D hardness				Surface Roughness							
	vPLA		rPLA		vPLA		rPLA					
	Level	Description	Level		Description		Level	Description	Level		Description	
Layer Height (mm)	3	0.3	3		0.3		1	0.1	1		0.1	
Infill (%)	3	100	3		100		1	60	2		60	
Nozzle Temperature (°C)	3	215	3		215		2	205	2		205	

3.9 DoE confirmation test

The optimal parameters resulting in the most favourable mechanical properties for the vPLA and rPLA specimens have been summarised in Table 9. A confirmation experiment was conducted to validate the potential of the optimised parameter conditions determined by Taguchi analysis to improve the mechanical properties. The test was necessary to validate the conditions suggested by the Taguchi analysis, which resulted in the optimal properties. The predicted results for the optimal conditions were determined solely by considering the optimum performance factors. Confirmation test results for several mechanical properties, such as tensile strength, flexural strength, impact strength, shore D hardness, and surface roughness, were obtained using the optimal combination of factors, as listed in Table 9. The obtained results for these properties were found to be 61.25 MPa and 45.97 MPa for tensile strength, 104.05 MPa and 89.87 MPa for flexural strength, 5.61 and 5.37 kJ/m^2 for impact strength, 82.30 and 79.60 for shore D hardness, and 1.97 µm and 2.28 µm for surface roughness of vPLA and rPLA specimens, respectively. The results demonstrated that the samples produced using the optimal combination of factors exhibited higher levels of accuracy than those generated by the L9 orthogonal array. Therefore, the *S/N* ratio of the selected combination of factors was employed for $S/N_{\text{confirmation}}$.

The optimal combination of factors was determined by calculating the predicted values. The comparison between the confirmation test data and the predicted results is presented in Table 10. It is widely recognised in the engineering community that achieving a 95% confidence interval is a fundamental principle in engineering tests in order to ensure high-quality products and testing validity [102]. Therefore, the CI for both the confirmed and predicted outcomes were determined. For all the attributes listed in Table 10, the findings showed a significant degree of overlap between the CI obtained from the confirmation tests and predicted outcomes. A significant observation was made for the surface roughness property, as the experimental value showed a comparatively better result than the predicted value. The primary reason for this was the improvement in interlayer adhesion when the rPLA samples were printed using an optimal combination of printing parameters [17, 97]. This result suggests that the selected combination of factors in terms of material preparation and processing factors was acceptable and could be considered as optimal conditions during manufacturing. The ANOVA results suggested that the significant factors could be accurately predicted and combined to achieve good reproducibility.

Table 10 Confirmation test summary based on optimum factors

Output response		Prediction		Confirmation	
		$S/N_{predicted}$	$C.I_{predicted}$	$S/N_{confirmation}$	$C.I_{confirmation}$
Tensile strength	vPLA	35.80	±2.54	35.81	±0.21
	rPLA	32.21	±2.07	33.11	±1.21
Flexural strength	vPLA	39.74	±6.48	40.34	±1.45
	rPLA	39.43	±8.44	39.07	±1.47
Impact strength	vPLA	14.75	±0.31	14.97	±0.12
	rPLA	14.12	±0.26	14.60	±0.13
Shore D hardness	vPLA	38.21	±0.96	38.23	±1.41
	rPLA	37.62	±1.14	38.07	±1.12
Surface roughness	vPLA	−14.11	±2.12	−5.90	±0.17
	rPLA	−15.35	±2.37	−7.19	±0.14

4 Conclusions

The present study employed vPLA and rPLA filaments to investigate the influence of the layer thickness, infill percentage, and nozzle temperature on 3D printed specimen surface roughness, hardness, tensile, flexural, and Charpy impact properties. This study used the Taguchi L9 OA method to design the experiments, whilst the obtained results were additionally analysed by ANOVA to determine the optimal printing parameters for maximising the mechanical strength of recycled PLA specimens. The experimental results indicated that vPLA possessed overall stronger mechanical properties compared to rPLA at all the selected printing factors. The rPLA specimen properties exhibited lower overall results than the vPLA for the same layer thickness and nozzle temperature, but the former with a high layer thickness and high nozzle temperature could attain almost the same property as the latter. The main effect plots show that the tensile and flexural strengths exhibited the highest values when the layer thickness and nozzle temperature were high. ANOVA analysis also indicated that layer thickness had the highest significance amongst the input variables, with p values below 0.05, for all responses. In addition, the temperature of the nozzle also played a significant influence in enhancing the tensile characteristics. In contrast, the infill density had an insignificant influence on the range of values encountered in this study (60–100%). The optimum printing parameters for FDM using vPLA and rPLA filament based on ANOVA results for tensile, flexural, impact, and shore D hardness tests were 0.3 mm layer thickness, 215 ℃ nozzle temperature, and 100% infill density with the values for surface roughness being 0.1 mm, 205 ℃, and 80%, respectively. The results revealed that for a high layer height, infill amount, and nozzle temperature, the bonding between layers increased, which also had a beneficial effect on the mechanical strength. Microscopic investigations showed that a high nozzle temperature and layer height resulted in a stronger microstructure. In contrast to this, the existence of voids was observed when the temperature was low (195 ℃), causing a reduction in mechanical properties. Finally, the predicted responses for individual parameters were verified through experimental confirmation. These additional experiments showed that using the optimally determined printing parameters, rPLA achieved a high tensile strength of 45.97 MPa, which was comparable to the tensile strength of vPLA when printed with 0.1 mm layer thickness, 215 °C nozzle temperature, and 80% infill density. Therefore, the experimental investigation proved that rPLA could be a feasible environmentally friendly alternative material for virgin PLA owing to the similarity of its mechanical properties under optimum processing conditions. Since this study evaluated the optimal printing parameters for the layer thickness, infill, and nozzle temperature of recycled PLA specimens, future research could focus on choosing other important printing parameters, such as printing speed, infill angle for the evaluation of mechanical properties, and determining the fatigue properties of vPLA and rPLA specimens. The investigation and minimisation of the residual stress could be an interesting field for future research. In addition, investigating the use of blends of recycled and virgin PLA may be useful in 3D printing in order to evaluate the resulting mechanical properties and attendant sustainability benefits.

Acknowledgements The authors are grateful to the technical staff of the School of Civil and Mechanical Engineering, Curtin University, Australia, for their valuable technical support.

Author contribution Experimentation, data curation, and writing the original draft: M.R.H; conceptualisation and methodology: all authors; writing, review, and editing: all authors.

Funding Open Access funding enabled and organized by CAUL and its Member Institutions.

Data availability All data generated or analysed during this study, along with associated materials, will be made available at Curtin Research Data Collection.

Declarations

Ethics approval and consent to participate The article followed the guidelines of the Committee on Publication Ethics (COPE) and involved no studies on human or animal subjects.

Consent for publication All authors read and approved the final manuscript.

Competing interests The authors declare no competing interests.

References

1. Abdullah Aloyaydi B, Sivasankaran S, Rizk Ammar H (2019) Influence of infill density on microstructure and flexural behavior of 3D printed PLA thermoplastic parts processed by fusion deposition modeling. AIMS Mater Sci 6:1033–1048. https://doi.org/10.3934/matersci.2019.6.1033
2. Jayawardane H, Davies IJ, Gamage JR, John M, Biswas WK (2023) Sustainability perspectives – a review of additive and subtractive manufacturing. Sustain Manuf Service Econ 2. https://doi.org/10.1016/j.smse.2023.100015
3. Pinho AC, Amaro AM, Piedade AP (2020) 3D printing goes greener: study of the properties of post-consumer recycled polymers for the manufacturing of engineering components. Waste Manag 118:426–434. https://doi.org/10.1016/j.wasman.2020.09.003
4. Farazin A, Mohammadimehr M (2021) Effect of different parameters on the tensile properties of printed polylactic acid samples by FDM: experimental design tested with MDs simulation. Int J Adv Manuf Technol 118:103–118. https://doi.org/10.1007/s00170-021-07330-w
5. Geyer R, Jambeck JR, Law KL (2017) Production, use, and fate of all plastics ever made. Sci Adv 3:e1700782. https://doi.org/10.1126/sciadv.1700782
6. Pulok MKH, Rahman MS, Chakravarty UK (2021) Crack Propagation and Fracture Toughness of Additively Manufactured Polymers. Proceedings of the ASME 2021 International Mechanical Engineering Congress and Exposition Volume 4: Advances in Aerospace Technology. Virtual, Online. November 1-5, 2021. ASME. https://doi.org/10.1115/imece2021-72061
7. Matsuzaki R, Ueda M, Namiki M, Jeong T-K, Asahara H, Horiguchi K, Nakamura T, Todoroki A, Hirano Y (2016) Three-dimensional printing of continuous-fiber composites by in-nozzle impregnation. Sci Rep 6:23058. https://doi.org/10.1038/srep23058
8. Jayawardane H, Davies IJ, Gamage JR, John M, Biswas WK (2022) Investigating the 'techno-eco-efficiency' performance of pump impellers: metal 3D printing vs. CNC machining. Int J Adv Manuf Technol 121:6811–6836. https://doi.org/10.1007/s00170-022-09748-2
9. Uddin MS, Sidek MFR, Faizal MA, Ghomashchi R, Pramanik A (2017) Evaluating mechanical properties and failure mechanisms of fused deposition modeling acrylonitrile butadiene styrene parts. J Manuf Sci Eng 139. https://doi.org/10.1115/1.4036713
10. Maguluri N, Suresh G, Rao KV (2023) Assessing the effect of FDM processing parameters on mechanical properties of PLA parts using Taguchi method. J Thermoplast Compos Mater 36:1472–1488. https://doi.org/10.1177/08927057211053036
11. Jayawardane H, Davies IJ, Leadbeater G, John M, Biswas WK (2021) 'Techno-eco-efficiency' performance of 3D printed impellers: an application of life cycle assessment. Int J Sustain Manuf 5. https://doi.org/10.1504/ijsm.2021.116871
12. Badia JD, Ribes-Greus A (2016) Mechanical recycling of polylactide, upgrading trends and combination of valorization techniques. Eur Polymer J 84:22–39. https://doi.org/10.1016/j.eurpolymj.2016.09.005
13. Sabil M, Prabhakar DAP (2022) Optimisation of extrusion temperature and infill density of PLA material by using L16 orthogonal array. Aust J Mech Eng 1–17. https://doi.org/10.1080/14484846.2022.2073022
14. Hikmat M, Rostam S, Ahmed YM (2021) Investigation of tensile property-based Taguchi method of PLA parts fabricated by FDM 3D printing technology. Results Eng 11:100264. https://doi.org/10.1016/j.rineng.2021.100264
15. Jayawardane H, Davies IJ, Gamage JR, John M, Biswas WK (2023) Additive manufacturing of recycled plastics: a 'techno-eco-efficiency' assessment. Int J Adv Manuf Technol 126:1471–1496. https://doi.org/10.1007/s00170-023-11169-8
16. Torres J, Cole M, Owji A, Demastry Z, Gordon AP (2016) An approach for mechanical property optimization of fused deposition modeling with polylactic acid via design of experiments. Rapid Prototyp J 22:387–404. https://doi.org/10.1108/rpj-07-2014-0083
17. Atakok G, Kam M, Koc HB (2022) Tensile, three-point bending and impact strength of 3D printed parts using PLA and recycled PLA filaments: a statistical investigation. J Market Res 18:1542–1554. https://doi.org/10.1016/j.jmrt.2022.03.013
18. Taib N-AAB, Rahman MR, Huda D, Kuok KK, Hamdan S, Bakri MKB, Julaihi MRMB, Khan A (2022) A review on poly lactic acid (PLA) as a biodegradable polymer. Polym Bull 80:1179–1213. https://doi.org/10.1007/s00289-022-04160-y
19. Zhao XG, Hwang K-J, Lee D, Kim T, Kim N (2018) Enhanced mechanical properties of self-polymerized polydopamine-coated recycled PLA filament used in 3D printing. Appl Surf Sci 441:381–387. https://doi.org/10.1016/j.apsusc.2018.01.257
20. Cruz Sanchez FA, Boudaoud H, Hoppe S, Camargo M (2017) Polymer recycling in an open-source additive manufacturing

context: mechanical issues. Addit Manuf 17:87–105. https://doi.org/10.1016/j.addma.2017.05.013
21. Singh S, Singh M, Prakash C, Gupta MK, Mia M, Singh R (2019) Optimization and reliability analysis to improve surface quality and mechanical characteristics of heat-treated fused filament fabricated parts. Int J Adv Manuf Technol 102:1521–1536. https://doi.org/10.1007/s00170-018-03276-8
22. Tan WS, Tanoto YY, Jonoadji N, Christian AA (2021) The effect of cooling and temperature in 3D printing process with fused deposition modelling technology on the mechanical properties with polylactic acid recycled material. Int Rev Mech Eng 15. https://doi.org/10.15866/ireme.v15i12.21573
23. Ahmad MN, Ishak MR, Mohammad Taha M, Mustapha F, Leman Z, Anak Lukista DD, Irianto Ghazali I (2022) Application of Taguchi method to optimize the parameter of fused deposition modeling (FDM) using oil palm fiber reinforced thermoplastic composites. Polymers (Basel) 14. https://doi.org/10.3390/polym14112140
24. Dey A, Hoffman D, Yodo N (2020) Optimizing multiple process parameters in fused deposition modeling with particle swarm optimization. Int J Interact Des Manuf 14:393–405. https://doi.org/10.1007/s12008-019-00637-9
25. Correia C, Gomes TEP, Gonçalves I, Neto V (2022) Reprocessability of PLA through chain extension for fused filament fabrication. J Manuf Mater Process 6:26. https://doi.org/10.3390/jmmp6010026
26. Breški T, Hentschel L, Godec D, Đuretek I (2021) Suitability of recycled PLA filament application in fused filament fabrication process. Tehnički glasnik 15:491–497. https://doi.org/10.31803/tg-20210805120621
27. Subramaniyan M, Karuppan S, Eswaran P, Appusamy A, Naveen Shankar A (2021) State of art on fusion deposition modeling machines process parameter optimization on composite materials. Mater Today: Proc 45:820–827. https://doi.org/10.1016/j.matpr.2020.02.865
28. Lanzotti A, Grasso M, Staiano G, Martorelli M (2015) The impact of process parameters on mechanical properties of parts fabricated in PLA with an open-source 3-D printer. Rapid Prototyp J 21:604–617. https://doi.org/10.1108/rpj-09-2014-0135
29. Eryildiz M (2021) Effect of build orientation on mechanical behaviour and build time of FDM 3D-printed PLA parts: an experimental investigation. Eur Mech Sci 5:116–120. https://doi.org/10.26701/ems.881254
30. Benamira M, Benhassine N, Ayad A, Dekhane A (2023) Investigation of printing parameters effects on mechanical and failure properties of 3D printed PLA. Eng Fail Anal 148. https://doi.org/10.1016/j.engfailanal.2023.107218
31. Tsouknidas A, Pantazopoulos M, Katsoulis I, Fasnakis D, Maropoulos S, Michailidis N (2016) Impact absorption capacity of 3D-printed components fabricated by fused deposition modelling. Mater Des 102:41–44. https://doi.org/10.1016/j.matdes.2016.03.154
32. Carneiro OS, Silva AF, Gomes R (2015) Fused deposition modeling with polypropylene. Mater Des 83:768–776. https://doi.org/10.1016/j.matdes.2015.06.053
33. Kam M, İpekci A, Şengül Ö (2021) Taguchi optimization of fused deposition modeling process parameters on mechanical characteristics of PLA+ filament material. Scientia Iranica. https://doi.org/10.24200/SCI.2021.57012.5020
34. Suteja TJ, Soesanti A (2020) Mechanical properties of 3D printed polylactic acid product for various infill design parameters: a review. J Phys: Conf Ser 1569. https://doi.org/10.1088/1742-6596/1569/4/042010
35. Behzadnasab M, Yousefi AA, Ebrahimibagha D, Nasiri F (2019) Effects of processing conditions on mechanical properties of PLA printed parts. Rapid Prototyp J 26:381–389. https://doi.org/10.1108/rpj-02-2019-0048
36. Sun Q, Rizvi GM, Bellehumeur CT, Gu P (2008) Effect of processing conditions on the bonding quality of FDM polymer filaments. Rapid Prototyp J 14:72–80. https://doi.org/10.1108/13552540810862028
37. Heidari-Rarani M, Ezati N, Sadeghi P, Badrossamay MR (2020) Optimization of FDM process parameters for tensile properties of polylactic acid specimens using Taguchi design of experiment method. J Thermoplast Compos Mater 35:2435–2452. https://doi.org/10.1177/0892705720964560
38. Maazinejad B, Mohammadnia O, Ali GAM, Makhlouf ASH, Nadagouda MN, Sillanpää M, Asiri AM, Agarwal S, Gupta VK, Sadegh H (2020) Taguchi L9 (34) orthogonal array study based on methylene blue removal by single-walled carbon nanotubes-amine: adsorption optimization using the experimental design method, kinetics, equilibrium and thermodynamics. J Mol Liq 298. https://doi.org/10.1016/j.molliq.2019.112001
39. Chari VS, Venkatesh P, Krupashankar K, Dinesh V (2018) Effect of processing parameters on FDM process. AIP Conference Proceedings. AIP Publishing. https://doi.org/10.1063/1.5029637
40. Sood AK, Ohdar RK, Mahapatra SS (2012) Experimental investigation and empirical modelling of FDM process for compressive strength improvement. J Adv Res 3:81–90. https://doi.org/10.1016/j.jare.2011.05.001
41. Aa A, Qattawi A, Alrawi B, Guzman A (2017) Experimental optimization of fused deposition modelling processing parameters: a design-for-manufacturing approach. Procedia Manuf 10:791–803. https://doi.org/10.1016/j.promfg.2017.07.079
42. Freeland B, McCarthy E, Balakrishnan R, Fahy S, Boland A, Rochfort KD, Dabros M, Marti R, Kelleher SM, Gaughran J (2022) A review of polylactic acid as a replacement material for single-use laboratory components. Materials 15. https://doi.org/10.3390/ma15092989
43. Auffray L, Gouge P-A, Hattali L (2022) Design of experiment analysis on tensile properties of PLA samples produced by fused filament fabrication. Int J Adv Manuf Technol 118:4123–4137. https://doi.org/10.1007/s00170-021-08216-7
44. Lokesh N, Praveena BA, Sudheer Reddy J, Vasu VK, Vijaykumar S (2022) Evaluation on effect of printing process parameter through Taguchi approach on mechanical properties of 3D printed PLA specimens using FDM at constant printing temperature. Mater Today: Proc 52:1288–1293. https://doi.org/10.1016/j.matpr.2021.11.054
45. Hanon MM, Dobos J, Zsidai L (2021) The influence of 3D printing process parameters on the mechanical performance of PLA polymer and its correlation with hardness. Procedia Manuf 54:244–249. https://doi.org/10.1016/j.promfg.2021.07.038
46. Park K, Kim G, No H, Jeon HW, Kremer GEO (2020) Identification of optimal process parameter settings based on manufacturing performance for fused filament fabrication of CFR-PEEK. Appl Sci 10. https://doi.org/10.3390/app10134630
47. Oloyede CT, Jekayinfa SO, Alade AO, Ogunkunle O, Laseinde OT, Adebayo AO, Abdulkareem AI, Smaisim GF, Fattah IMR (2023) Synthesis of biobased composite heterogeneous catalyst for biodiesel production using simplex lattice design mixture: optimization process by Taguchi method. Energies 16. https://doi.org/10.3390/en16052197
48. Mrabti IE, Bouziane K, Touache A, Hakimi AE, Chamat A, Daya A (2022) Effect of process parameters on the deep drawing formability of aluminum and advanced high-strength steel square cups. Int J Adv Manuf Technol 124:1827–1842. https://doi.org/10.1007/s00170-022-10616-2
49. Boswell B, Islam MN, Davies IJ, Pramanik A (2015) Effect of machining parameters on the surface finish of a metal matrix

composite under dry cutting conditions. Proc Inst Mech Eng Part B: J Eng Manuf 231:913–923. https://doi.org/10.1177/0954405415583776
50. ASTM-D638-22 (2022) Standard test method for tensile properties of plastics. ASTM International. West Conshohocken, PA, United States. https://doi.org/10.1520/D0638-22
51. Ramesh M, Panneerselvam K (2020) PLA-Based Material Design and Investigation of Its Properties by FDM. In: Shunmugam MS, Kanthababu M (eds) Advances in Additive Manufacturing and Joining. Lecture Notes on Multidisciplinary Industrial Engineering. Springer, Singapore. pp. 229–241. https://doi.org/10.1007/978-981-32-9433-2_20
52. ASTM-D618-21 (2021) Standard practice for conditioning plastics for testing. ASTM International. West Conshohocken, PA, United States. https://doi.org/10.1520/d0618-21
53. Kim G, Barocio E, Tsutsui W, Wang P, Dubikovsky S, Pipes RB, Sterkenburg R (2021) Enhancing surface characteristics of additively manufactured fiber reinforced thermoplastic mold using thermoset coating with ceramic particles. Surf Coat Technol 422. https://doi.org/10.1016/j.surfcoat.2021.127536
54. ASTM-D2240-15 (2021) Standard test method for rubber property-durometer hardness. ASTM International. West Conshohocken, PA, United States. https://doi.org/10.1520/d2240-15r21
55. Chand R, Sharma VS, Trehan R, Gupta MK, Sarikaya M (2023) Investigating the dimensional accuracy and surface roughness for 3D printed parts using a multi-jet printer. J Mater Eng Perform 32:1145–1159. https://doi.org/10.1007/s11665-022-07153-0
56. Bouzaglou O, Golan O, Lachman N (2023) Process design and parameters interaction in material extrusion 3D printing: a review. Polymers (Basel) 15. https://doi.org/10.3390/polym15102280
57. Mishra P, Sood S, Bharadwaj V, Aggarwal A, Khanna P (2023) Parametric modeling and optimization of dimensional error and surface roughness of fused deposition modeling printed polyethylene terephthalate glycol parts. Polymers (Basel) 15. https://doi.org/10.3390/polym15030546
58. Gadelmawla ES, Koura MM, Maksoud TMA, Elewa IM, Soliman HH (2002) Roughness parameters. J Mater Process Technol 123:133–145. https://doi.org/10.1016/s0924-0136(02)00060-2
59. Lalegani Dezaki M, Ariffin MKAM, Serjouei A, Zolfagharian A, Hatami S, Bodaghi M (2021) Influence of infill patterns generated by CAD and FDM 3D printer on surface roughness and tensile strength properties. Appl Sci 11:7272. https://doi.org/10.3390/app11167272
60. Fly D, Açan M (2013) 3D Printed Internal Structure: Influence on Tensile Strength. 2013 North Midwest Section Meeting. Fargo, North Dakota. October 17-18, 2013. ASEE. https://doi.org/10.18260/1-2-1139-36234
61. ASTM-D7127-17 (2017) Standard test method for measurement of surface roughness of abrasive blast cleaned metal surfaces using a portable stylus instrument. ASTM International. West Conshohocken, PA, United States. https://doi.org/10.1520/d7127-17
62. Maidin S, Fadani I, Md. Nor Hayati N, Albaluooshi H, (2022) Application of Taguchi method to optimize fused deposition modeling process parameters for surface roughness. J Teknol 84:29–37. https://doi.org/10.11113/jurnalteknologi.v84.18430
63. ASTM-E4 (2021) Standard practices for force calibration and verification of testing machines. ASTM International. West Conshohocken, PA, United States. https://doi.org/10.1520/e0004-21
64. ASTM-D790-17 (2017) Standard test methods for flexural properties of unreinforced and reinforced plastics and electrical insulating materials. ASTM International. West Conshohocken, PA, United States. https://doi.org/10.1520/D0790-17
65. Chandrasekaran C (2017) 19 - Testing of Rubber Lining. In: Chandrasekaran C (ed) Anticorrosive Rubber Lining. William Andrew Publishing. pp. 165–172. https://doi.org/10.1016/B978-0-323-44371-5.00019-0
66. ASTM-D6110-18 (2018) Standard test method for determining the charpy impact resistance of notched specimens of plastics. ASTM International. West Conshohocken, PA, United States. https://doi.org/10.1520/d6110-18
67. Popelka A, Zavahir S, Habib S (2020) Morphology analysis. In: AlMaadeed MAA, Ponnamma D, Carignano MA (eds) Polymer Science and Innovative Applications. Elsevier. pp. 21–68. https://doi.org/10.1016/b978-0-12-816808-0.00002-0
68. Vidakis N, David C, Petousis M, Sagris D, Mountakis N (2023) Optimization of key quality indicators in material extrusion 3D printing of acrylonitrile butadiene styrene: the impact of critical process control parameters on the surface roughness, dimensional accuracy, and porosity. Mater Today Commun 34. https://doi.org/10.1016/j.mtcomm.2022.105171
69. Kim YJA (2014) The Effect of Surface Roughness on Biofilm Adhesion to Clear Heat-cured Poly (methyl Methacrylate) used for Ocular Prostheses. Master of Health Sciences, University of Otago. [Online]. Available: http://hdl.handle.net/10523/4792
70. Kackar RN (1989) Taguchi's quality philosophy: analysis and commentary. In: Dehnad K (ed) Quality Control, Robust Design, and the Taguchi Method. Springer, US Boston, MA, pp 3–21
71. Peace GS (1993) Taguchi methods: a hands-on approach. Addison Wesley Publishing Company
72. Phadke MS, Kackar RN, Speeney DV, Grieco MJ (1989) Off-line quality control in integrated circuit fabrication using experimental design. In: Dehnad K (ed) Quality Control, Robust Design, and the Taguchi Method. Springer, US Boston, MA, pp 99–141
73. Dehnad K (2012) Quality control, robust design, and the Taguchi method Springer New York, NY
74. Tamizharasan T, Senthilkumar N, Selvakumar V, Dinesh S (2019) Taguchi's methodology of optimizing turning parameters over chip thickness ratio in machining P/M AMMC. SN Appl Sci 1. https://doi.org/10.1007/s42452-019-0170-8
75. Ross PJ (1988) Taguchi techniques for quality engineering: loss function, orthogonal experiments, parameter and tolerance design. McGraw-Hill
76. Chen W-H, Carrera Uribe M, Kwon EE, Lin K-YA, Park Y-K, Ding L, Saw LH (2022) A comprehensive review of thermoelectric generation optimization by statistical approach: Taguchi method, analysis of variance (ANOVA), and response surface methodology (RSM). Renew Sustain Energy Rev 169. https://doi.org/10.1016/j.rser.2022.112917
77. Anderson MJ (2001) A new method for non-parametric multivariate analysis of variance. Austral Ecol 26:32–46. https://doi.org/10.1111/j.1442-9993.2001.01070.pp.x
78. Yang WH, Tarng YS (1998) Design optimization of cutting parameters for turning operations based on the Taguchi method. J Mater Process Technol 84:122–129. https://doi.org/10.1016/s0924-0136(98)00079-x
79. Rizk TH (2023) Chapter 31 - Analysis of variance. In: Eltorai AEM, Liu T, Chand R, Kalva SP (eds) Translational Interventional Radiology. Academic Press. pp. 149–152. https://doi.org/10.1016/B978-0-12-823026-8.00024-9
80. Greenwald AG, Gonzalez R, Harris RJ, Guthrie D (1996) Effect sizes and p values: what should be reported and what should be replicated? Psychophysiology 33:175–183. https://doi.org/10.1111/j.1469-8986.1996.tb02121.x
81. Belavendram N (1995) Quality by design: taguchi techniques for industrial experimentation. Prentice Hall
82. Bikas H, Stavropoulos P, Chryssolouris G (2015) Additive manufacturing methods and modelling approaches: a critical review. Int J Adv Manuf Technol 83:389–405. https://doi.org/10.1007/s00170-015-7576-2

83. Mani M, Karthikeyan AG, Kalaiselvan K, Muthusamy P, Muruganandhan P (2022) Optimization of FDM 3-D printer process parameters for surface roughness and mechanical properties using PLA material. Mater Today: Proc 66:1926–1931. https://doi.org/10.1016/j.matpr.2022.05.422
84. Ayrilmis N (2018) Effect of layer thickness on surface properties of 3D printed materials produced from wood flour/PLA filament. Polym Testing 71:163–166. https://doi.org/10.1016/j.polymertesting.2018.09.009
85. Shirmohammadi M, Goushchi SJ, Keshtiban PM (2021) Optimization of 3D printing process parameters to minimize surface roughness with hybrid artificial neural network model and particle swarm algorithm. Prog Addit Manuf 6:199–215. https://doi.org/10.1007/s40964-021-00166-6
86. Zeng YS, Hsueh MH, Lai CJ, Hsiao TC, Pan CY, Huang WC, Chang CH, Wang SH (2022) An investigation on the hardness of polylactic acid parts fabricated via fused deposition modeling. Polymers (Basel) 14. https://doi.org/10.3390/polym14142789
87. Maguluri N, Suresh G, Guntur SR (2022) Effect of printing parameters on the hardness of 3D printed poly-lactic acid parts using DOE approach. IOP Conf Ser: Mater Sci Eng 1248. https://doi.org/10.1088/1757-899x/1248/1/012004
88. Şirin Ş, Aslan E, Akincioğlu G (2022) Effects of 3D-printed PLA material with different filling densities on coefficient of friction performance. Rapid Prototyp J 29:157–165. https://doi.org/10.1108/rpj-03-2022-0081
89. Hsueh MH, Lai CJ, Liu KY, Chung CF, Wang SH, Pan CY, Huang WC, Hsieh CH, Zeng YS (2021) Effects of printing temperature and filling percentage on the mechanical behavior of fused deposition molding technology components for 3d printing. Polymers (Basel) 13. https://doi.org/10.3390/polym13172910
90. Lanzotti A, Martorelli M, Maietta S, Gerbino S, Penta F, Gloria A (2019) A comparison between mechanical properties of specimens 3D printed with virgin and recycled PLA. Procedia CIRP 79:143–146. https://doi.org/10.1016/j.procir.2019.02.030
91. Dave HK, Prajapati AR, Rajpurohit SR, Patadiya NH, Raval HK (2020) Open hole tensile testing of 3D printed parts using in-house fabricated PLA filament. Rapid Prototyp J 26:21–31. https://doi.org/10.1108/rpj-01-2019-0003
92. Dong Y, Milentis J, Pramanik A (2018) Additive manufacturing of mechanical testing samples based on virgin poly (lactic acid) (PLA) and PLA/wood fibre composites. Adv Manuf 6:71–82. https://doi.org/10.1007/s40436-018-0211-3
93. Puchalski M, Kwolek S, Szparaga G, Chrzanowski M, Krucinska I (2017) Investigation of the influence of PLA molecular structure on the crystalline forms (alpha' and alpha) and mechanical properties of wet spinning fibres. Polymers (Basel) 9. https://doi.org/10.3390/polym9010018
94. Kumar S, Singh R, Singh TP, Batish A (2019) Flexural, pull-out, and fractured surface characterization for multi-material 3D printed functionally graded prototype. J Compos Mater 54:2087–2099. https://doi.org/10.1177/0021998319892067
95. Thoden van Velzen EU, Chu S, Alvarado Chacon F, Brouwer MT, Molenveld K (2020) The impact of impurities on the mechanical properties of recycled polyethylene. Packag Technol Sci 34:219–228. https://doi.org/10.1002/pts.2551
96. Kamaal M, Anas M, Rastogi H, Bhardwaj N, Rahaman A (2020) Effect of FDM process parameters on mechanical properties of 3D-printed carbon fibre–PLA composite. Prog Addit Manuf 6:63–69. https://doi.org/10.1007/s40964-020-00145-3
97. Syrlybayev D, Zharylkassyn B, Seisekulova A, Akhmetov M, Perveen A, Talamona D (2021) Optimisation of strength properties of FDM printed parts-a critical review. Polymers (Basel) 13. https://doi.org/10.3390/polym13101587
98. Tao Y, Kong F, Li Z, Zhang J, Zhao X, Yin Q, Xing D, Li P (2021) A review on voids of 3D printed parts by fused filament fabrication. J Market Res 15:4860–4879. https://doi.org/10.1016/j.jmrt.2021.10.108
99. Akhoundi B, Nabipour M, Hajami F, Shakoori D (2020) An experimental study of nozzle temperature and heat treatment (annealing) effects on mechanical properties of high-temperature polylactic acid in fused deposition modeling. Polym Eng Sci 60:979–987. https://doi.org/10.1002/pen.25353
100. Shahavi MH, Hosseini M, Jahanshahi M, Meyer RL, Darzi GN (2015) Clove oil nanoemulsion as an effective antibacterial agent: Taguchi optimization method. Desalin Water Treat 57:18379–18390. https://doi.org/10.1080/19443994.2015.1092893
101. Fazita RN, Johary N, Khalil HPSA, Norazli N, Azniwati A, Haafiz MKM (2021) Parameter optimization via the Taguchi method to improve the mechanical properties of bamboo particle reinforced polylactic acid composites. BioResources 16:1914–1939. https://doi.org/10.15376/biores.16.1.1914-1939
102. Salam H, Dong Y, Davies IJ, Pramanik A (2018) Identification of preferred combination of factors in manufacturing bioepoxy/clay nanocomposites. Adv Compos Mater 27:511–530. https://doi.org/10.1080/09243046.2018.1480147